

# Lawrence Berkeley National Laboratory

## Recent Work

### Title

Recent Progress and Perspective in Electrode Materials for K-Ion Batteries

### Permalink

<https://escholarship.org/uc/item/4pg85349>

### Journal

Advanced Energy Materials, 8(9)

### ISSN

1614-6832

### Authors

Kim, H  
Kim, JC  
Bianchini, M  
[et al.](#)

### Publication Date

2018-03-26

### DOI

10.1002/aenm.201702384

Peer reviewed

# Recent Progress and Perspective in Electrode Materials for K-Ion Batteries

Haegyeom Kim, Jae Chul Kim, Matteo Bianchini, Dong-Hwa Seo, Jorge Rodriguez-Garcia, and Gerbrand Ceder\*

The development of rechargeable batteries using K ions as charge carriers has recently attracted considerable attention in the search for cost-effective and large-scale energy storage systems. In light of this trend, various materials for positive and negative electrodes are proposed and evaluated for application in K-ion batteries. Here, a comprehensive review of ongoing materials research on nonaqueous K-ion batteries is offered. Information on the status of new materials discovery and insights to help understand the K-storage mechanisms are provided. In addition, strategies to enhance the electrochemical properties of K-ion batteries and computational approaches to better understand their thermodynamic properties are included. Finally, K-ion batteries are compared to competing Li and Na systems and pragmatic opportunities and future research directions are discussed.

## 1. Introduction

Energy consumption in modern society has been continuously increasing. The International Energy Outlook 2016 (IEO 2016) prepared by the U.S. Energy Information Administration estimates that the world energy consumption will grow by 48% between 2012 and 2040.<sup>[1]</sup> With concerns over depleting fossil fuels as well as global warming, it is critical to utilize renewable energy resources. Indeed, wind, solar, and geothermal resources are becoming the world's fastest-growing sources for power generation. IEO 2016 also reports that renewable-energy-generated power will increase by an average of 2.6% annually through 2040.<sup>[1]</sup> However, renewable energy is inherently intermittent, creating a discrepancy between energy harvesting

and demand in terms of time and space. Thus, grid-level stationary energy storage systems (ESSs) play a key role in making renewable energies both effective and efficient and thereby shaping a more sustainable and environmental friendly society.

Although different energy storage technologies including mechanical, electrical, chemical, and electrochemical systems have been proposed,<sup>[2,3]</sup> mechanical energy storage through pumped hydroelectricity currently dominates the market ( $\approx 95\%$  of the installed capacity,  $\approx 183$  GW).<sup>[4]</sup> Electrochemical energy storage is also being considered as a promising option for ESSs based on its flexibility of deployment with little restriction on size and geographical location, low maintenance costs,

large energy density, high round-trip efficiency, and long cycle life.<sup>[3,5,6]</sup>


The market for Li-ion batteries (LIBs), originally commercialized for portable electronic devices (i.e., cell phones and laptops), is now expanding to electric vehicles (EVs) and grid-level ESSs. However, it remains debatable whether the global Li reserves,  $\approx 14$  million tons, can meet the increasing demand for such large-scale applications.<sup>[7–9]</sup> The price of lithium carbonate, which is a primary precursor for LIBs, has been continuously increasing since 2000,<sup>[10]</sup> and this trend is likely to accelerate once the EV and ESS markets take off. Moreover, Li is geographically limited to specific regions:  $\approx 86\%$  of the Li reserves are located in Bolivia, Chile, China, Argentina, and Australia;<sup>[9]</sup> therefore, geopolitical issues may arise. A more pressing issue for Li-ion markets is the use of Co in all high-energy-density systems. With more than 50% of all mined Co destined for use in Li-ion technology, and a substantial fraction of that coming from the Democratic Republic of the Congo, Li-ion growth may be hampered by the availability of Co.<sup>[11]</sup> As a less expensive alternative to LIBs, Na-ion batteries (NIBs) have been extensively studied.<sup>[6,12–14]</sup> The relatively high standard redox potential of Na/Na<sup>+</sup> leads to a lower working voltage and thereby lower energy density than Li-ion. In addition, hard carbon, which is associated with a high production cost and low material's density, must be used as an anode in NIBs, as graphite, which is the standard anode for LIBs, cannot store Na ions.<sup>[15–17]</sup>

Recently, K-ion batteries (KIBs) have emerged as another possible energy storage system.<sup>[18–20]</sup> It is notable that the abundance of K resources in the Earth's crust and oceans is similar to that of Na (Figure 1a).<sup>[21,22]</sup> The cost of potassium carbonate

Dr. H. Kim, Dr. J. C. Kim, Dr. M. Bianchini, Prof. G. Ceder  
Materials Sciences Division  
Lawrence Berkeley National Laboratory  
Berkeley, CA 94720, USA  
E-mail: gceder@berkeley.edu

Dr. D.-H. Seo, Prof. G. Ceder  
Department of Materials Science and Engineering  
University of California  
Berkeley, CA 94720, USA

J. Rodriguez-Garcia  
Instituto Nacional del Carbon (INCAR)  
Francisco Pintado Fe, 26, 33011 Oviedo, Asturias, Spain

 The ORCID identification number(s) for the author(s) of this article can be found under <https://doi.org/10.1002/aenm.201702384>.

DOI: 10.1002/aenm.201702384

(≈1000 USD per ton) is also much lower than that of lithium carbonate (≈6500 USD per ton).<sup>[23,24]</sup> More importantly, K has a lower standard redox potential than Na and even Li in non-aqueous electrolytes, which can be translated into a potentially higher cell voltage of KIBs compared with those of NIBs and LIBs.<sup>[25,26]</sup> The most important advantage of KIB technology over NIB technology is that graphite can accommodate reversible K de/intercalation.<sup>[26]</sup> In addition, Okoshi et al. showed that K electrolytes exhibit higher conductivity than Li and Na electrolytes.<sup>[27]</sup> These authors attributed the higher conductivity to the smaller Stokes radius of solvated K ions due to its weak Lewis acidity, and to the low interfacial reaction resistance resulting from the small desolvation activation energy.<sup>[27]</sup> Given these advantages, KIBs have rapidly attracted considerable interest, and various materials have been developed and evaluated as potential KIB electrodes (Figure 1b,c).

In this review, we present an overview of recent experimental and computational achievements as well as an outlook for nonaqueous KIBs, focusing on the development of new negative and positive electrodes and their underlying K storage mechanisms. For anodes, we concentrate on K-intercalation in graphite and its electrochemical properties; briefly discuss the alternative anode materials including hard carbon, K intercalation compounds, K metal-alloying-reaction compounds, K conversion-reaction compounds, organic compounds. We also emphasize the development of promising cathode materials, including Prussian blue analogues, layered compounds, poly-anions, and organic materials, and provide perspectives on electrode materials for KIBs in a broader context.

## 2. Anode Materials

The development of post-Li-ion technologies has largely been motivated by the necessity to overcome the limits of LIBs in terms of performance and cost. The latter, in particular, has raised increasing concern as the price of Li precursors has steeply increased in the last few years.<sup>[28,29]</sup> The lower price of sodium carbonate has therefore driven a large body of research on NIBs.<sup>[12,30]</sup> Recently, interest in KIBs has been sparked by a development on the anode side, i.e., the fact that K, unlike Na, can intercalate into graphite. This section will include research on negative electrode materials for KIBs, including graphite, various forms of carbon, metal alloys, intercalation compounds, organics, and conversion anodes.

### 2.1. Graphite Anodes

K-graphite intercalated compounds (K-GICs) have been reported in the literature since the 1950s.<sup>[31,32]</sup> These compounds were prepared using non-electrochemical methods, through a two-zone vapor transport method, which applies K vapor onto graphite in a custom-made double furnace. Several compounds were isolated in these studies from stage 1 to stage 5 of potassiation,<sup>[33]</sup> with stage 1 corresponding to the most K-rich compound, KC<sub>8</sub>. Analogous to the case of Li-GICs, one refers to an *n*th stage compound to indicate insertion of an intercalate layer into every *n*th graphite interlayer space.



**Haegyom Kim** received a Ph.D. degree (2015) on graphite derivatives for Li and Na rechargeable batteries at Seoul National University. Currently, he is a postdoctoral fellow in Prof. Gerbrand Ceder's group at Lawrence Berkeley National Laboratory. His research interest lies in the development of next-generation energy storage materials and systems. His current research focuses on the development of novel electrode materials for high-energy alkali ion batteries, including Li, Na, and K ion batteries.



**Jae Chul Kim** is a materials postdoc fellow at Lawrence Berkeley National Laboratory working with Prof. Gerbrand Ceder. He has a broad interest in materials and interface design for electrochemical systems, and his current research focuses on the development of next generation energy storage technologies including energy-dense alkali-ion batteries, as well as their all-solid-state systems. He obtained his Ph.D. under the supervision of Prof. Ceder in Materials Science and Engineering at the Massachusetts Institute of Technology (MIT), where he performed in-depth investigation to understand electrochemical and structural properties of Li battery materials.



**Matteo Bianchini** is a postdoctoral researcher at Lawrence Berkeley National Lab in the group of Prof. Gerbrand Ceder, working on synthesis and characterization of new materials for next-generation batteries. After his studies in physics engineering at Politecnico di Milano, he obtained a Ph.D. in France in 2015, a collaboration between ILL (Grenoble), LRCS (Amiens), and ICMCB (Bordeaux). He worked on operando diffraction experiments using neutrons, X-rays, and synchrotron radiation to study Li-ion and Na-ion battery electrode materials.

A recent density functional theory (DFT) study compared the intercalation of Li, Na, and K into graphite.<sup>[34]</sup> The authors found that the intercalation of Na is indeed energetically unfavorable,

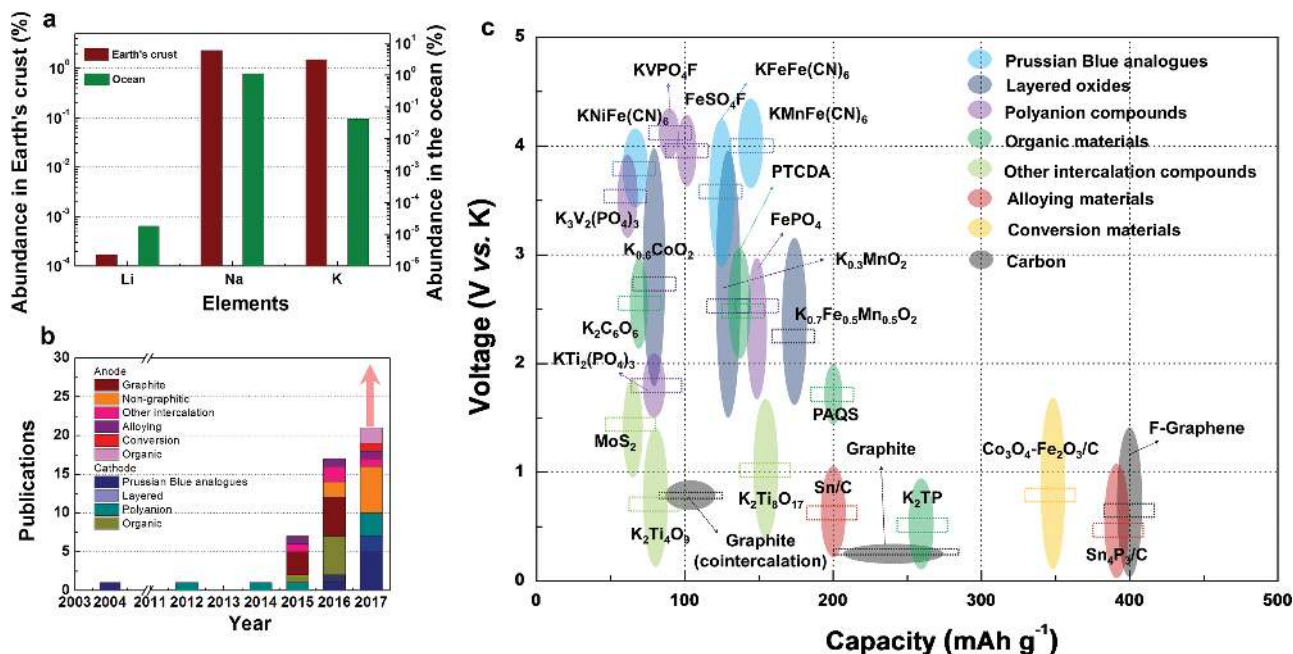


**Figure 1.** a) Abundance of Li, Na, and K.<sup>[21,22]</sup> b) Number of publications on electrode materials for KIBs according to Google Scholar (accessed May 26, 2017). c) Capacity versus voltage plots of electrode materials for KIBs reported to date (as of May 26, 2017).

unlike that of Li. More interestingly, K intercalation is even more favorable than that of Li (with formation enthalpies for  $\text{KC}_8$  and  $\text{LiC}_6$  of  $-27.5$  and  $-16.5$  kJ mol<sup>-1</sup>, respectively).

Consistent with these computations, Komaba et al.<sup>[26]</sup> and Jian et al.<sup>[35]</sup> demonstrated that electrochemical intercalation of K into graphite in a KIB cell is possible. **Figure 2** illustrates the main features of this process. A large 1st discharge capacity was reported, with a 1st cycle reversibility strongly dependent on the electrode's formulation (consistent with the role of the solid-electrolyte interphase (SEI) as discussed in the following). After the 1st cycle, graphite consistently delivered a capacity as high as 273 mA h g<sup>-1</sup> (vs the theoretical capacity of 279 mA h g<sup>-1</sup>, calculated using the molecular weight of  $\text{KC}_8$  as the most potassiated phase). Plateaus are observed close to 0.1–0.17 and 0.27–0.32 V during potassiation and depotassiation, respectively, with a typical polarization of 0.1–0.2 V. **Figure 2a–d** also compares Li and K cells. Overall, K intercalates at higher voltage than Li, consistent with its more negative formation energy.<sup>[10]</sup> In addition, for K intercalation a large peak is centered at 0.32 V with two shoulders at 0.41 and 0.52 V instead of the three definite processes at 0.23, 0.16, and 0.12 V for Li intercalation, leading to a smooth voltage curve at high voltage. The higher average voltage for K insertion into graphite as compared to Li can lower the energy density of a full cell. However, a higher anode voltage is also beneficial as it reduces the risk of metal plating under high rate or low-T conditions, when Li plating is highly problematic.

Jian et al.<sup>[35]</sup> confirmed the known K-graphite intercalation compounds (K-GICs) using ex situ X-ray diffraction (XRD) on electrochemically discharged samples. They observed the reversible sequence C– $\text{KC}_{36}$ – $\text{KC}_{24}$ – $\text{KC}_8$  (**Figure 2e,f**), indicating that the stage 3, 2, and 1 compounds crystallized in a sequence analogous to the crystallization of the phases prepared by the two-zone vapor method,<sup>[31,32]</sup> except that the stage 4 and 5

compounds were not detected electrochemically. This discrepancy could originate from the fact that ex situ diffraction was only performed on a limited number of samples (i.e., nonoperando conditions) and it is easy to miss phases that exist in a narrow composition range. Note that for the stage 1 compound, K is regularly arranged in the center of carbon hexagons in every layer, forming an arrangement with a nominal composition of  $\text{KC}_8$ . For stage 2, K ions occupy every other layer, and the K content in each K-filled layer is found to be two thirds of that of the stage 1 phase; the composition of stage 2 compound then becomes  $\text{K}_{2/3}\text{C}_{16}$  (i.e.,  $\text{KC}_{24}$ ), rather than  $\text{KC}_{16}$ .<sup>[32]</sup> The ex situ experiments also revealed a large volume expansion upon potassiation, corresponding to an increase in the unit cell parameter  $c$  of  $\approx 60\%$  (3.35–5.35 Å). Nonetheless, reversibility of the graphite peak during cycling was observed, indicating that exfoliation of the material does not occur.

A large volume expansion is often blamed for poor capacity retention upon cycling. Komaba et al.<sup>[26]</sup> showed that the cell configuration and, in particular, the selection of binder and electrolyte are crucial to obtain good 1st cycle efficiency and capacity retention. Their work thoroughly compares the use of different binders coupled with graphite. As observed in **Figure 3**, the use of different binders results in significant differences in the electrochemical performance. Replacing polyvinylidene difluoride (PVDF) with sodium polyacrylate (PANa) drastically improves the 1st cycle coulombic efficiency, cycle stability, and rate capability. In particular, its use results in impressive rate performance (230 mA h g<sup>-1</sup> retained at 15 C–4.2 A g<sup>-1</sup>), as shown in **Figure 3d**. However, a large amount of the literature published after this work still uses PVDF as the functional binder, which results in many reports claiming improved performance achieved by various forms of carbon, but only over this poorly chosen baseline.

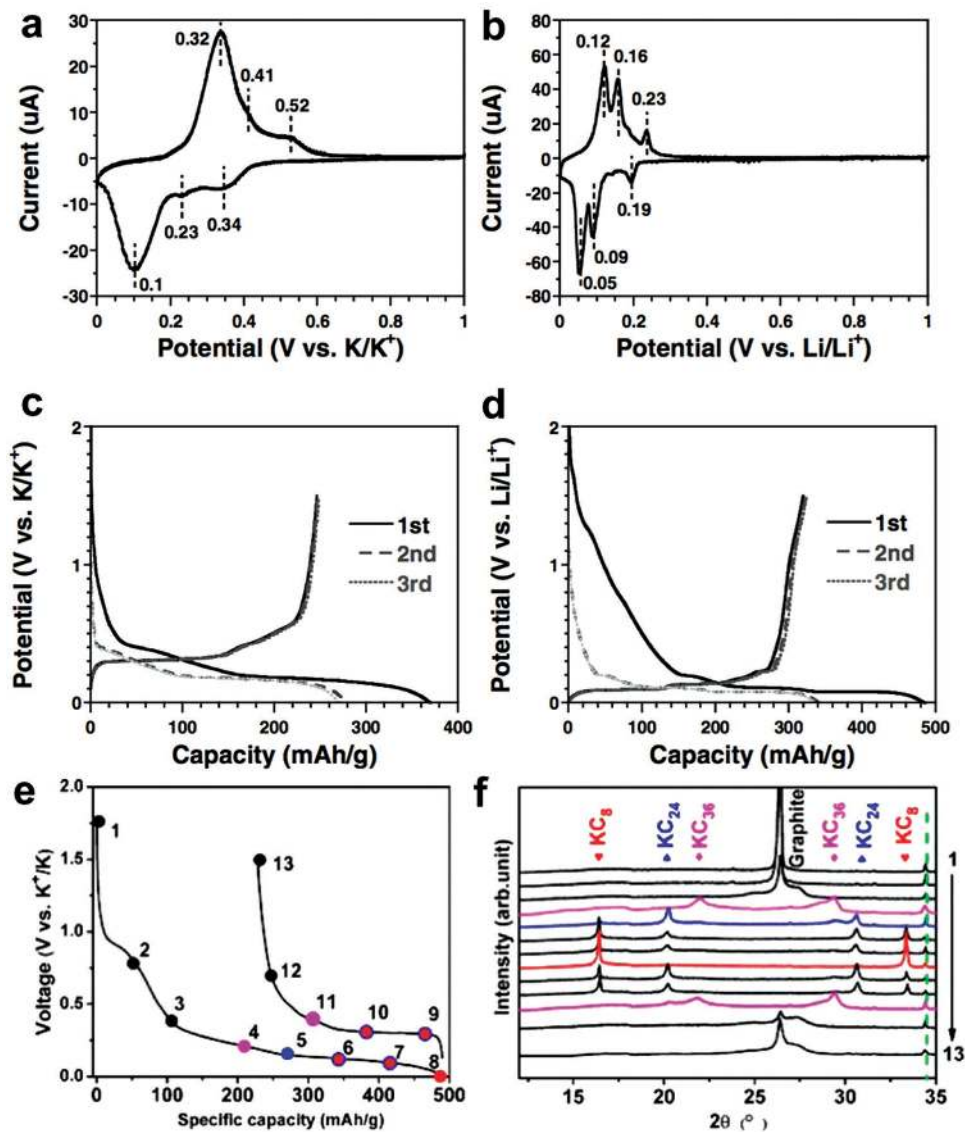


**Figure 2.** a,b) Cyclic voltammery curves and c,d) charge/discharge voltage profiles of graphite in (a,c) KIBs and (b,d) LIBs cycled versus metal in EC:PC electrolytes. Reproduced with permission.<sup>[36]</sup> Copyright 2016, WILEY-VCH. e) 1st cycle voltage–capacity profile of a K-graphite cell cycled at C/10. f) XRD patterns of electrodes corresponding to the marked state of charges in (e). Reproduced with permission.<sup>[35]</sup> Copyright 2015, American Chemical Society.

In addition, Zhao et al.<sup>[36]</sup> showed that the electrolyte can critically influence whether stable SEI layers form. Evaluating 1 M KPF<sub>6</sub> in ethylene carbonate:dimethyl carbonate (EC:DMC), EC:diethyl carbonate (EC:DEC), and EC:propylene carbonate (EC:PC) electrolytes in K metal | graphite + Na alginate (binder) cells they found that EC:DMC results in poor performance. They attribute this to the lack of stable SEI formation as in DMC-containing electrolytes severe and continuous decomposition occurred. By contrast, EC:DEC (which is used in most of KIB literature) and EC:PC worked well with the graphite anode, resulting in more than 200 reversible cycles. The use of EC:PC resulted in slightly better capacity retention and higher 1st cycle coulombic efficiency.

Xu et al.<sup>[37]</sup> computed the intrinsic mobility of K in graphite using a dispersion-corrected density functional (DFT-D2). The authors analyzed the kinetics in various real and artificial

K-GICs (KC<sub>8n</sub> (*n* = 1, 2, 3) and KC<sub>12n</sub> (*n* = 1, 2)) by estimating the defect energies and activation energies for K migration. In the K-GICs, the activation energies for K migration by the vacancy mechanism is low (*E*<sub>a</sub> = 0.16–0.27 eV) while the activation energies for K migration by a Frenkel mechanism is very high (2.42 eV). Although these activation energies for K migration were calculated on very few data points along the K displacement path, the values reported by the authors are undoubtedly low and indicate good K kinetics. In fact, the authors claimed that all the activation energies for K migration via the vacancy mechanism are lower than those of Li in Li-GICs based on comparison of their values with those of Thinius et al.<sup>[38]</sup> Thus, migration through the vacancy mechanism likely indicates good K mobility in graphite, at least comparable to Li (the values reported by Xu et al. are indeed quite similar to those reported by Persson et al.).<sup>[39]</sup>

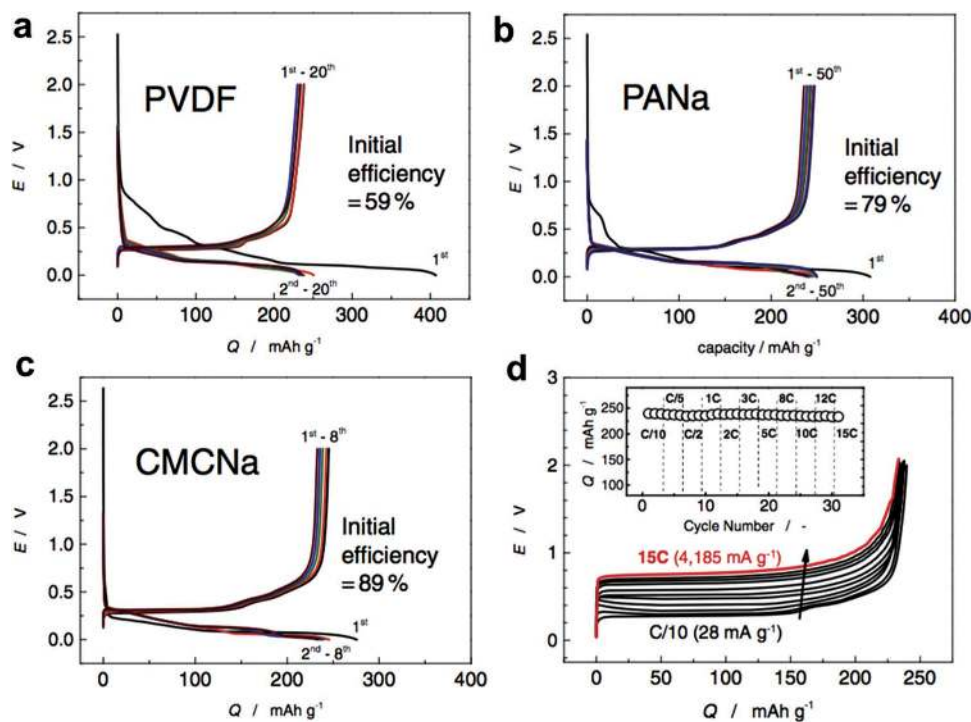


**Figure 3.** Charge–discharge curves of graphite electrode formed on Al foil with a) PVDF, b) PANa, and c) carboxymethyl cellulose (CMC) binders in 1 M potassium bis(fluorosulfonyl)imide (KFSI) in EC:DEC for K cells. d) Oxidation rate capability of the PANa electrode. Reproduced with permission.<sup>[26]</sup> Copyright 2015, Elsevier.

Although the above theoretical study suggests comparable kinetics of K and Li ions in graphite and the measured mobility of K in the electrolyte is higher than that of Li,<sup>[26]</sup> Li-graphite cells perform “better” in experiments, namely they have lower polarization and resistance.<sup>[36]</sup> This may imply that the interface and SEI resistances are larger in the K-graphite cell. Thus, engineering of the electrode and electrolyte compositions is a key to obtaining high rate capabilities in graphite-based negative electrodes in KIBs.

## 2.2. Other Carbon Anodes

Similarly to the findings reported for Na,<sup>[40]</sup> several forms of carbon other than graphite have been reported to successfully intercalate K, including soft carbon,<sup>[35]</sup> hard carbon microspheres,<sup>[41]</sup> hard–soft composites,<sup>[42]</sup> N-doped hard carbon and carbon nanofibers,<sup>[43]</sup> pencil-trace carbon,<sup>[44]</sup> tire-derived carbon,<sup>[45]</sup> polynanocrystalline graphite,<sup>[46]</sup> reduced graphene oxide,<sup>[47]</sup> and F-, N-, P-, and O-doped, and undoped graphene.<sup>[48–51]</sup> Most of these materials exhibit remarkable capacities, even in excess of the theoretical capacity of graphite. N-doped and F-doped graphenes are demonstrated to deliver close to 350 mA h g<sup>-1</sup>.<sup>[48,50]</sup> Their rate capability and capacity retention are fair (Table 1) but not as good as those obtained with graphite and PANa by Komaba et al. (230 mA h g<sup>-1</sup> at a 15 C rate), as shown in Figure 3d.<sup>[26]</sup> Chen et al.<sup>[43]</sup> reported a N-doped carbon material with high rate capability using nongraphitic carbon: 154 mA h g<sup>-1</sup> at a 72 C rate. In this case the authors argue from their CV curves that instead of true intercalation, a mainly surface-driven adsorption reaction is

responsible for the electrochemical activity. In addition, Jian et al.<sup>[42]</sup> demonstrated that the limited rate capability of hard carbon and the capacity fading of soft carbon can be overcome by forming hard–soft composites, merging the best aspects of both materials. Tai et al. and Adams et al. prepared self-standing films of carbon nanofibers or graphene<sup>[44,52]</sup> to avoid the use of binders, which simplifies the SEI chemistry and results in remarkable long-term cycling stability (1900 cycles at 1 C rate).

Carbon anodes can also be synthesized using waste or scrap materials derived from waste tires,<sup>[45]</sup> seafood waste (chitin),<sup>[43]</sup> or pencils.<sup>[44]</sup> The idea of recycling waste materials to produce anodes for KIBs is interesting and may help to reduce battery fabrication costs. Finally, co-intercalation using glyme-based solvents has also been demonstrated for KIBs,<sup>[53,54]</sup> analogous to the work performed for NIBs.<sup>[16]</sup>

In conclusion, several authors proved the storage of K ions into nongraphitic carbonaceous anodes, and showed they can deliver satisfactory performances in terms of specific capacity and rate capability. However, practically the nongraphitic carbonaceous anodes are unlikely to rival graphite, especially from a volumetric energy density standpoint. Nonetheless, some of these nongraphitic carbonaceous anodes can be produced from waste materials and presumably at very low cost, so it is possible that they will find application in low-cost KIB full cells.

## 2.3. Alloying Anodes

Alloying of alkali metals with other elements has been regarded as a potential route to prepare high-capacity anodes for Li<sup>[55,56]</sup>

**Table 1.** Electrochemical performance of graphite- and carbon-based negative electrodes for KIBs.

Reference	Anode type	Binder and carbon additive	Electrolyte	1st K insertion [mA h g <sup>-1</sup> ]	1st K extraction [mA h g <sup>-1</sup> ]	Initial coulombic efficiency	Capacity retention	Best rate capability [mA h g <sup>-1</sup> ]
Jian et al. <sup>[35]</sup>	Graphite	PVDF	0.8 M KPF <sub>6</sub> in EC:DEC	475	273	57.4%	51% (50 cycles)	80 at 1 C
	Soft carbon			≈540	273	≈50%	81.4% (50 cycles)	140 at 5 C (1.4 A g <sup>-1</sup> )
Komaba et al. <sup>[26]</sup>	Graphite	PVDF	1 M KFSI in EC:DEC	≈400	≈220	59%	Negligible fade (20 cycles)	–
		PANa		≈310	244	79%	Negligible fade (50 cycles)	≈230 at 15 C (4.2 A g <sup>-1</sup> )
		CMCNa		≈280	≈230	89%	Negligible fade (8 cycles)	–
Luo et al. <sup>[47]</sup>	Graphite	PVDF	0.5 M KPF <sub>6</sub> in EC:DEC	280	207	74.3%	–	141 at 200 mA g <sup>-1</sup>
	Reduced graphene oxide	None		442	222	50.2%	150 mA h g <sup>-1</sup> (170 cycles)	50 at 100 mA g <sup>-1</sup>
Jiang and co-workers <sup>[37]</sup>	Hard carbon microspheres	Carbon additive + PVDF	0.8 M KPF <sub>6</sub> in EC:DEC	≈300	262	≈87.3%	83% (100 cycles)	136 at 5 C
Zhao et al. <sup>[36]</sup>	Graphite	Na alginate	1 M KPF <sub>6</sub> in EC:DEC	≈480	≈225	47%	200 mA h g <sup>-1</sup> (200 cycles)	–
			1 M KPF <sub>6</sub> in EC:DMC	≈510	≈220	42.7%	Failure after 140 cycles	–
			1 M KPF <sub>6</sub> in EC:PC	370	246	66.5%	220 mA h g <sup>-1</sup> (200 cycles)	110 at 100 mA g <sup>-1</sup>
			PVDF	1 M KPF <sub>6</sub> in EC:PC	≈540	≈240	44.5%	200 mA h g <sup>-1</sup> (15 cycles)
Ju et al. <sup>[48]</sup>	F-doped graphene foam	Super P + PVDF	0.8 M KPF <sub>6</sub> in EC:DEC	864	355.6	41.2%	166 mA h g <sup>-1</sup> (200 cycles)	212 at 500 mA g <sup>-1</sup>
Cohn et al. <sup>[53]</sup>	Graphite	Carbon black + PVDF	1 M KPF <sub>6</sub> in monoglyme	≈120	80	67%	80 mA h g <sup>-1</sup> (15 cycles)	–
		Carbon black + PVDF	1 M KPF <sub>6</sub> in diglyme	≈137	100	73%	100 mA h g <sup>-1</sup> (15 cycles)	–
Co-intercalation	Graphene foam	None	1 M KPF <sub>6</sub> in diglyme	100	99	99%	95% (1000 cycles)	80 at 100 C
Share et al. <sup>[49]</sup>	Few-layer graphene	None	0.8 M KPF <sub>6</sub> in EC:DEC	≈450	≈215	≈47%	140 mA h g <sup>-1</sup> (100 cycles)	60 at 100 mA g <sup>-1</sup>
Xing et al. <sup>[46]</sup>	Poly nanocrystalline graphite	C black + CMC	0.8 M KPF <sub>6</sub> in EC:DEC	414	224	54.1%	50% (240 cycles)	43.2 at 1000 mA g <sup>-1</sup>
Share et al. <sup>[50]</sup>	N-doped graphene	None	0.8 M KPF <sub>6</sub> in EC:DEC	≈640	350	55%	210 mA h g <sup>-1</sup> (100 cycles)	50 at 200 mA g <sup>-1</sup>
Li et al. <sup>[45]</sup>	Tire-derived carbon	10% PVDF + 10% Super C65 carbon	0.8 M KPF <sub>6</sub> in EC:DEC	≈600	192	37.1%	155 mA h g <sup>-1</sup> (200 cycles)	60 at 2 C
Tai et al. <sup>[44]</sup>	Pencil-trace carbon	None (also no current collector)	0.8 M KPF <sub>6</sub> in EC:DEC	≈290	≈190	65.5%	75% (350 cycles)	0.4 at 1.1 mA g <sup>-1</sup>
Ma et al. <sup>[51]</sup>	P- and O-doped graphene	10% PVDF + 20% black acetylene	1 M KClO <sub>4</sub> in EC:DEC	2504	566	22%	385 mA h g <sup>-1</sup> (600 cycles)	160 at 2 A g <sup>-1</sup>
Chen et al. <sup>[43]</sup>	N-rich hard carbon	10% PVDF	0.8 M KPF <sub>6</sub> in EC:DEC	–	250	–	180 mA h g <sup>-1</sup> (4000 cycles at 1.8 C)	154 at 72 C
Jian et al. <sup>[42]</sup>	Hard–soft carbon composite	10% CMC + 10% carbon	0.8 M KPF <sub>6</sub> in EC:DEC	389	261	67%	200 mA h g <sup>-1</sup> (200 cycles)	81 at 10 C
Adams et al. <sup>[52]</sup>	N- and O-rich carbon nanofibers	None	0.8 M KPF <sub>6</sub> in EC:DEC	≈600	≈245	41%	170 mA h g <sup>-1</sup> (1900 cycles at 1 C)	110 at 10 C

and Na batteries.<sup>[13]</sup> These anodes exploit the ability of certain elements to alloy with Li, Na, and K, leading to substantially higher achievable specific capacity compared with those of carbon-based anodes. **Figure 4a** shows which elements alloy with Li, Na, or K. Similar to Li and Na, K alloys with several elements, including Si, P, Ge, Sn, Sb, and Pb. Among those more heavily investigated in the past, Sb is attractive because of its reasonably low cost and its ability to alloy up to composition  $\text{Li}_3\text{Sb}$  (or  $\text{Na}_3\text{Sb}$ ), resulting in a capacity of  $660 \text{ mA h g}^{-1}$ . Similar alloys are known to form with K, leading to the natural choice of the K–Sb system as a potential anode material. In addition, Sn is well known for its ability to alloy with Li and Na, forming  $\text{Li}_{4.4}\text{Sn}$  and  $\text{Na}_{15}\text{Sn}_4$  compounds with theoretical capacities of 991 and  $845 \text{ mA h g}^{-1}$ , respectively. Finally, red phosphorous is one of the most promising anode materials for NIBs.<sup>[30]</sup> Similar to Na and unlike Li, K does not alloy with Al, potentially enabling its use as a less expensive current collector on the anode than Cu.

Using first-principles DFT calculations, we computed and compared the energetics of alloying K and Na (A) with different anode materials (M) known to alloy with Na, such as Si, P, Ge,

Sn, Sb, and Pb. The average voltage was calculated from the ground-state DFT energies as<sup>[10]</sup>

$$\langle \bar{V} \rangle = - \frac{E(A_{x_1}M_y) - E(A_{x_2}M_y) - (x_2 - x_1)E(A)}{(x_2 - x_1)F} \quad (1)$$

where  $E(A_{x_i}M_y)$  are the DFT energies of the most stable  $A_xM_y$  configurations at each composition and  $E(A)$  is the energy of the metal A. **Figure 4b** compares the alloying voltages of A with M to form  $A_xM$ . Two general trends are observed: first, the amount of K that can be alloyed is less than or equal to that of Na, indicating that the capacities of the K alloying anodes are generally expected to be smaller than those of their Na counterparts. Second, for almost all of the alloying reactions, the average voltage for K is higher than that for Na, except for partial states of reaction in P and Sb. This higher voltage leads to a loss of energy density for K systems. Note that the higher average voltage but lower capacity for K may at first seem at odds with each other, since the maximum capacity is set by the composition where the voltage reaches zero. Hence, one might expect a higher alloying capacity for K. But the higher average

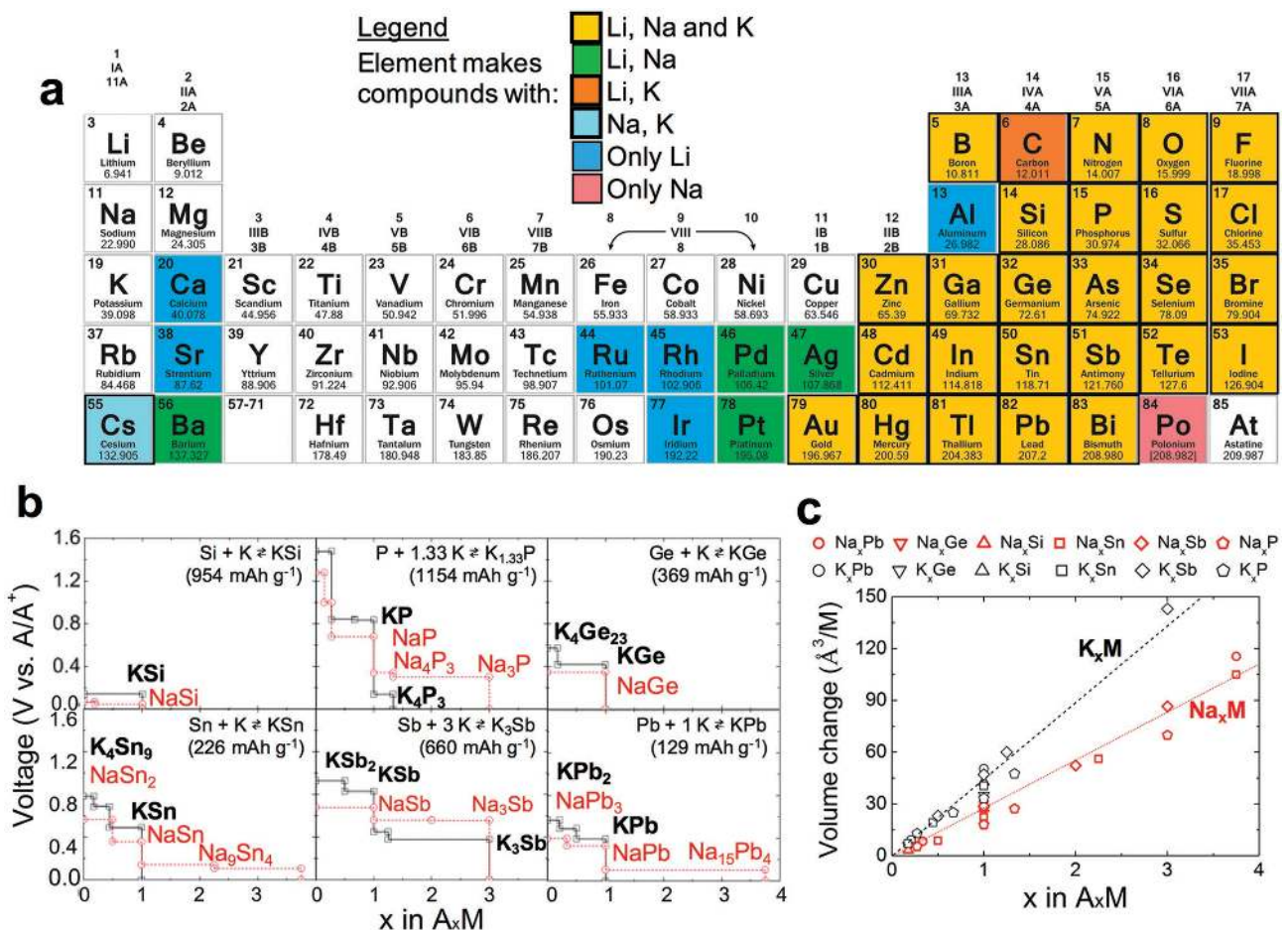


**Figure 4.** a) Extract of periodic table showing the elements that alloy or make compounds with Li, Na, and K. Only compounds whose existence has been shown with certainty have been included, as gathered from the literature.<sup>[59]</sup> b) Voltage–composition curves calculated for alkali alloying with different metals. Note that  $K_3P$  is reported in the literature but is not included in our figure because it is slightly unstable based on our 0 K DFT calculations. c) Volume expansion upon alloying alkali metals with different metals as a function of x in  $A_xM$ .



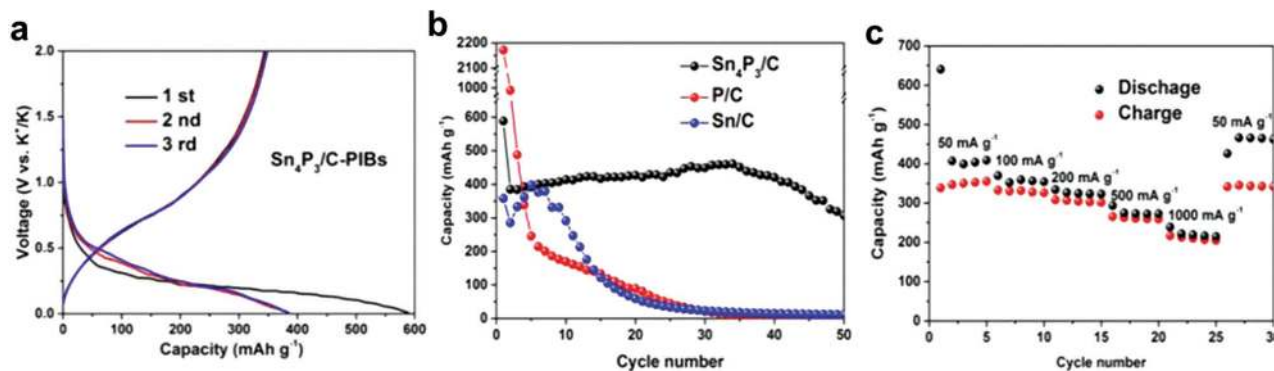


**Figure 5.** a) First three discharge/charge profiles of  $\text{Sn}_4\text{P}_3/\text{C}$  in KIB at a current density of  $50 \text{ mA g}^{-1}$ . b) Cycling performance of the  $\text{Sn}_4\text{P}_3/\text{C}$ ,  $\text{Sn}/\text{C}$ , and  $\text{P}/\text{C}$  electrodes in KIBs at a current density of  $50 \text{ mA g}^{-1}$ . c) Rate performance of  $\text{Sn}_4\text{P}_3/\text{C}$  electrode in KIBs at current densities ranging from 50 to  $1000 \text{ mA g}^{-1}$ . Reproduced with permission.<sup>[62]</sup> Copyright 2017, American Chemical Society.

voltage of K is accompanied by an average larger voltage slope for alloying K with metals. This leads the voltage curve to reach 0 V at smaller capacity than for Na. A similarly high slope for K was observed in layered cathode materials.<sup>[57,58]</sup>

In Figure 4c, we also compare the volume expansions computed for the K and Na alloying anodes. The volume expansion for the K system is substantially larger than that for the Na system because of the larger size of K. To make the K alloying anodes competitive, morphology optimization (the introduction of high porosity or nanostructuring) should be considered to prevent particle pulverization upon cycling.

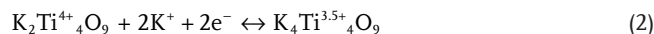
K alloying reactions have been experimentally observed for Sb, Sn, and P, and the results agree well with our computations. McCulloch et al. demonstrated that a Sb–C composite anode, in which C acts as a buffer layer to accommodate the large volume change, reversibly alloys with K for up to 10 cycles, forming cubic  $\text{K}_3\text{Sb}$  with a capacity of  $\approx 650 \text{ mA h g}^{-1}$ .<sup>[60]</sup> Unlike Li–Sn and Na–Sn alloys, which can alloy up to  $\text{Li}_{4.4}\text{Sn}$  and  $\text{Na}_{15}\text{Sn}_4$ , our DFT calculation predicts that K can alloy with Sn only up to a one-to-one ratio to produce the end-member  $\text{KSn}$  with a capacity of  $226 \text{ mA h g}^{-1}$ . Sultana et al. reported that a ball-milled Sn–graphite nanocomposite anode for KIBs<sup>[61]</sup> sustained a capacity of  $150\text{--}170 \text{ mA h g}^{-1}$  for  $\approx 10\text{--}15$  cycles, whereas bulk Sn is electrochemically inactive. The potassiumated phases were determined to likely be  $\text{K}_2\text{Sn}_5$  and  $\text{K}_4\text{Sn}_{23}$  based on ex situ XRD characterization. Phosphorus has a high theoretical capacity of  $2594 \text{ mA h g}^{-1}$  assuming that  $\text{K}_3\text{P}$  can be formed. Zhang et al.<sup>[62]</sup> investigated the electrochemical performance of P–C and  $\text{Sn}_4\text{P}_3\text{--C}$  composite anodes for KIBs. The P–C anode exhibited a high initial capacity (more than 2000 and  $1000 \text{ mA h g}^{-1}$  for the first two charge cycles), followed by an abrupt capacity fade, with retention of 9% of the capacity after 20 cycles. The results obtained for the  $\text{Sn}_4\text{P}_3\text{--C}$  composite anode are more promising, as shown in Figure 5. A reversible capacity of  $\approx 380 \text{ mA h g}^{-1}$  was achieved with an average voltage of  $\approx 0.5 \text{ V}$  over 50 cycles. In addition,  $\text{Sn}_4\text{P}_3\text{--C}$  exhibited good rate capability:  $\approx 385 \text{ mA h g}^{-1}$  at  $50 \text{ mA g}^{-1}$  and  $222 \text{ mA h g}^{-1}$  at  $1 \text{ A g}^{-1}$ . Importantly, this alloy retained a capacity of more than  $300 \text{ mA h g}^{-1}$  after 50 cycles.

Clearly, some metal alloying systems have shown promising enough initial performance for storing K at low voltage to warrant further investigation. However, from a cell energy density

perspective, the large volume expansion of K-alloying reactions will pose challenges, and as has been argued for Na,<sup>[13]</sup> it remains to be seen whether alloying can be competitive with intercalation anodes.

#### 2.4. Intercalation Anodes

Titanate-based compounds, including  $\text{Li}_4\text{Ti}_5\text{O}_{12}$ <sup>[63]</sup> and  $\text{Na}_3\text{Ti}_2\text{O}_7$ ,<sup>[64]</sup> have been widely investigated as nongraphitic intercalation anodes for Li and Na systems. For KIBs, Kishore et al. proposed the use of  $\text{K}_2\text{Ti}_4\text{O}_9$ , which has a layered structure with a interlayer spacing suitable to host  $\text{K}^+$ .<sup>[65]</sup> Its theoretical capacity is  $129 \text{ mA h g}^{-1}$  based on the reaction



The structure of  $\text{K}_2\text{Ti}_4\text{O}_9$  consists of layers of zig-zag ribbons of  $\text{TiO}_6$  octahedra joined together at the corners (Figure 6a). Even though the capacity of  $97 \text{ mA h g}^{-1}$  obtained at 0.2 C (Figure 6b) is rather poor compared with that of other anode materials, the large interlayer distance ( $8 \text{ \AA}$ ) induces a negligible volume change upon cycling, as observed from ex situ XRD characterization. Another titanate compound,  $\text{K}_2\text{Ti}_8\text{O}_{17}$ , was reported by Han et al.<sup>[66]</sup> with a similar but not identical framework to  $\text{K}_2\text{Ti}_4\text{O}_9$  (Figure 6d). In  $\text{K}_2\text{Ti}_8\text{O}_{17}$ , the stepped layered structure is formed by edge- and corner-sharing  $\text{TiO}_6$  octahedra, providing large interstitial spaces and open channels for  $\text{K}^+$  transport. The material was synthesized by a hydrothermal method combined with a subsequent annealing treatment, inducing a peculiar high-surface-area morphology. A discharge capacity of  $181.5 \text{ mA h g}^{-1}$  at  $20 \text{ mA g}^{-1}$  was reported between 0.01 and 3.0 V versus  $\text{K}^+/\text{K}$ , corresponding to approximately two-thirds of the theoretical capacity ( $300 \text{ mA h g}^{-1}$  assuming  $\text{K}_8\text{Ti}_8\text{O}_{17}$ ), as shown in Figure 6e,f.

A member of the NASICON (Na superionic conductors) family,  $\text{KTi}_2(\text{PO}_4)_3$  has also been studied as an anode for KIBs. Its structure is analogous to  $\text{NaTi}_2(\text{PO}_4)_3$  as proven by Rietveld refinement.<sup>[67]</sup> In general, the NASICON structure consists of basic “lantern units” composed of two  $\text{TiO}_6$  octahedra that corner-share with three  $\text{PO}_4$  tetrahedra. K ions can occupy the interstitial sites, which are sufficiently large to allow for further

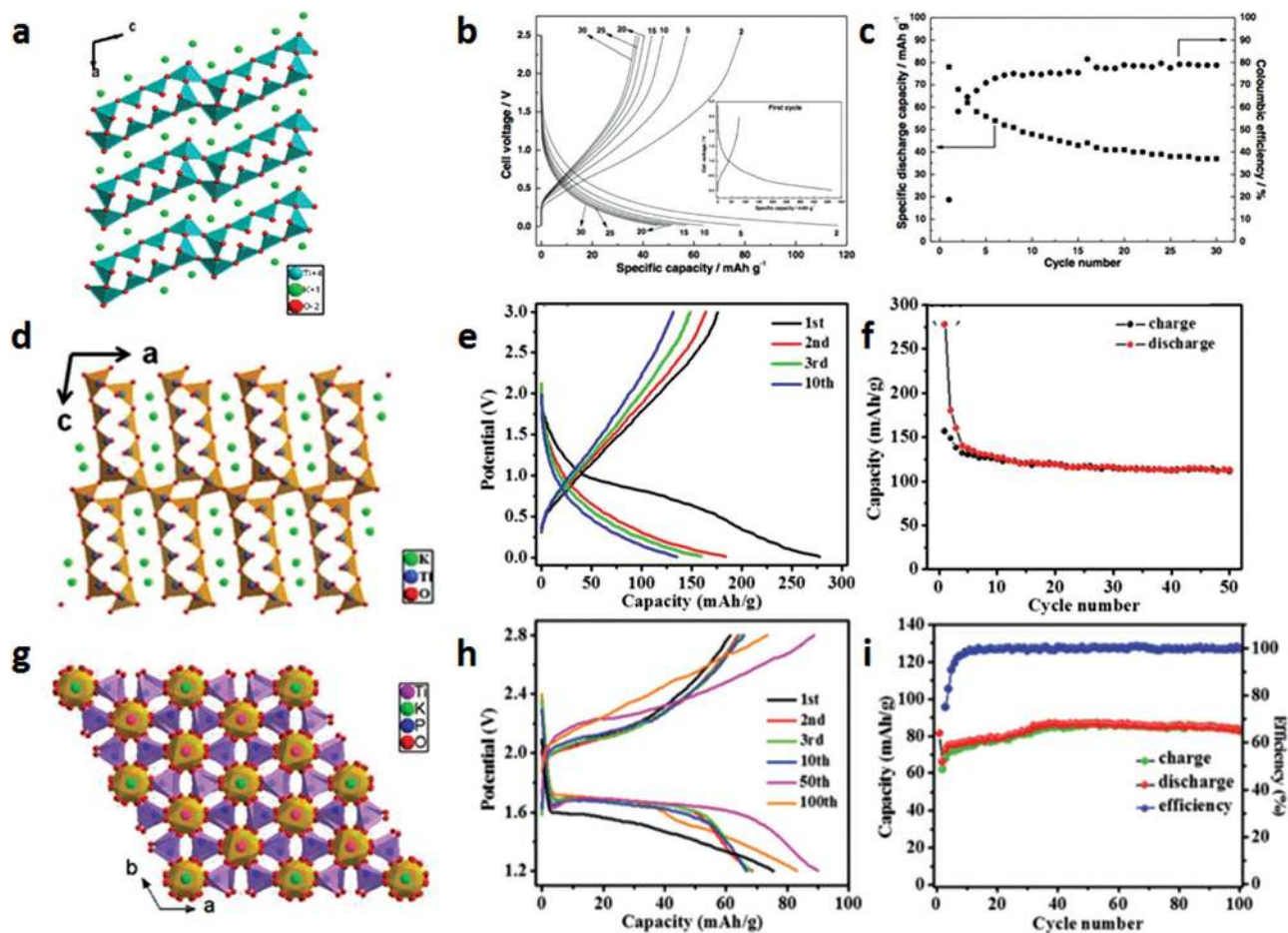


**Figure 6.** Top:  $K_2Ti_4O_9$ : a) crystal structure, b) galvanostatic charge–discharge curves for various cycles at  $100\text{ mA g}^{-1}$  ( $0.8\text{ C rate}$ ), and c) corresponding cycle life and coulombic efficiency. Reproduced with permission.<sup>[65]</sup> Copyright 2016, Electrochemical Society. Middle:  $K_2Ti_8O_{17}$ : d) crystal structure, e) 1st, 2nd, 3rd, and 10th discharge/charge curves at a current density of  $20\text{ mA g}^{-1}$  in the voltage range of  $0.01\text{--}3\text{ V}$  versus  $K^+/K$ , and f) cycling performance at a current density of  $20\text{ mA g}^{-1}$ . Reproduced with permission.<sup>[66]</sup> Copyright 2016, Royal Society of Chemistry. Bottom:  $KTi_2(PO_4)_3$ : g) crystal structure, h) discharge/charge curves at  $0.5\text{ C}$  ( $1\text{ C} = 128\text{ mA g}^{-1}$ ) versus  $K^+/K$ , i) and cycling performance at  $0.5\text{ C}$ . Reproduced with permission.<sup>[68]</sup> Copyright 2016, Royal Society of Chemistry.

K intercalation. Pure  $KTi_2(PO_4)_3$  with nanocubic morphology can be synthesized hydrothermally and coated with carbon to improve the electrical conductivity.<sup>[68]</sup> The theoretical capacity of one K insertion is  $127.7\text{ mA h g}^{-1}$ , which is achieved by reducing  $Ti^{4+}$  to  $Ti^{3.5+}$ . The carbon-coated material delivers  $75.6\text{ mA h g}^{-1}$  at  $0.5\text{ C}$  and  $42\text{ mA h g}^{-1}$  at  $11\text{ C}$  between  $1.2$  and  $2.8\text{ V}$  (Figure 6h). The discharge and charge plateaus are located at  $\approx 1.60$  and  $2.14\text{ V}$ , respectively, in the first discharge/charge curve. The good capacity retention observed over 100 cycles in Figure 6i has been attributed to the highly stable NASICON framework. While these results are promising, and it is reasonable to assume that the very high cycle life of some titanates as Li-anodes can be paralleled for K insertion, the relatively high voltage of these titanates is a significant limitation for their use in KIBs.

The only sulfur-based material reported as an anode for KIBs to date is  $MoS_2$ , which is a layered material, for which the intercalation properties have been extensively studied for select alkali and alkali-earth metals.<sup>[69]</sup> Ren et al. demonstrated K intercalation within the layers of  $MoS_2$ ,<sup>[70]</sup> as observed for other alkali metals.<sup>[71]</sup> After a first discharge of  $98\text{ mA h g}^{-1}$  (theoretical

capacity =  $167\text{ mA h g}^{-1}$ ), the capacity stabilized at  $\approx 65\text{ mA h g}^{-1}$  for 200 cycles. Using ex situ XRD, the authors showed that intercalation on an initial plateau at  $\approx 1.08\text{ V}$  corresponds to the formation of a  $K_{0.4}MoS_2$  phase, before reaching another small plateau at  $\approx 0.80\text{ V}$ . While more capacity could be obtained for  $K_xMoS_2$  ( $0.4 < x < 0.5$ ) in the sloped region at  $0.8\text{ V}$ , no change was observed in the XRD pattern except for a stronger intensity of the main (002) peak, which suggests the presence of a  $K_xMoS_2$  phase ( $0.4 < x < 0.5$ ) that remains layered. Discharge to a lower cut-off voltage leads to the formation of metallic Mo and  $K_xS$ . Note that the Li and Na counterparts are able to intercalate more than 0.4 per formula unit, resulting in a hexagonal-to-tetragonal phase transition at  $x \approx 0.5$  in  $Li_xMoS_2$  and  $Na_xMoS_2$ .

## 2.5. Organic Anodes

The use of organic molecules as anodes for KIBs was recently reported by Deng et al.<sup>[72]</sup> and Lei et al.<sup>[73]</sup> Dipotassium terephthalate ( $K_2TP$ ) and potassium 2,5-pyridinedicarboxylate ( $K_2PC$ )

are organic crystals built on a layered structure with  $K^+$  transport channels. Terephthalates, in particular, are well-known as anodes for LIBs and NIBs.<sup>[74,75]</sup> Although these small molecules crystallize in different space groups depending on the alkali species (A), they all react following a reaction  $A_2TP \rightarrow A_4TP$  upon discharge. Hence, their use as anodes for KIBs is based on the insertion of 2 K per molecule, resulting in a promising theoretical capacity of  $220 \text{ mA h g}^{-1}$ ; however, their low density is a drawback for practical applications. The oxidation/reduction capacity of these molecules is provided by gaining/losing electrons of the para-aromatic dicarboxylates while the  $K^+$  ions shuttle back and forth within the battery to maintain charge neutralization. They have been used in K-ion cells, delivering initial capacities of 270 and  $245 \text{ mA h g}^{-1}$  stabilizing at 181 and  $190 \text{ mA h g}^{-1}$  after 100 cycles, respectively. K insertion occurs through a plateau at 0.5 V for  $K_2TP$ , whereas a more sloped feature is observed for  $K_2PC$  between 0.7 and 0.5 V. Interestingly, 0.5 V for  $K_2TP$  is an intermediate value compared to the discharge voltage of  $Na_2TP$  (0.3 V) and  $Li_2TP$  (0.8 V). In situ XRD and Raman spectroscopy characterization revealed that upon K insertion toward  $K_4TP$  (or  $K_4PC$ ), the crystal structure was completely lost, resulting in the formation of an amorphous structure. Upon depotassiation, however, the crystal structure was almost entirely recovered. This is in part analogous to the behavior observed for  $Li_2TP$ : the material is crystalline at the end of the first discharge.<sup>[74]</sup> However, after 10 cycles to low voltage though, the material was shown to undergo amorphization.<sup>[76]</sup> Fourier-transform infrared spectroscopy and X-ray photoelectron spectroscopy studies also confirmed that the carboxylate group in  $K_2TP$  is responsible for the redox activity through the reduction of C=O bonds to C–O.

In the past, organic electrode materials have been plagued by the issue of solubility in the organic electrolyte, and by unanswered question of whether the reaction is proceeding in some cases through a dissolution/reprecipitation mechanism. However, in the case of TP there is no evidence for such detrimental mechanism, and the storage of alkali is carried out through a redox reaction. Also, further investigations are needed at this point to prove that organics can overcome their limitation of low specific energy, due to low material's density and to poor electrical conductivity, requiring high carbon content in the electrodes.<sup>[77,78]</sup>

## 2.6. Conversion Anodes

Negative electrodes that exploit the reduction of oxides to their metallic state—known as conversion anodes—are well-known for LIBs.<sup>[79]</sup> Recently, the use of a composite  $Co_3O_4$ – $Fe_2O_3$  as a conversion anode for KIBs was demonstrated.<sup>[80]</sup> The  $Co_3O_4$ – $Fe_2O_3$  nanoparticles dispersed in a Super P carbon matrix were prepared by magneto-ball-milling of molten-salt-synthesized nanoparticles of  $Co_3O_4$  and  $Fe_2O_3$  with Super P carbon black under a controlled atmosphere. This composite anode exhibited a reversible capacity of  $220 \text{ mA h g}^{-1}$  at  $50 \text{ mA g}^{-1}$  for 50 cycles, which is lower than that achieved for a similar material within Na cells ( $440 \text{ mA h g}^{-1}$ ). The average working potential of the  $Co_3O_4$ – $Fe_2O_3$ /C electrode in K cells is lower than those in Na and Li cells.

To summarize, the most meaningful finding in this early stage of research on anodes for KIBs has undoubtedly been K intercalation into graphite. Provided that appropriate binders and electrolytes are used, graphite demonstrates reasonable capacity, rate capability, and capacity retention. Although several other forms of carbon have been shown to store K ions, they are unlikely to rival graphite in terms of specific energy. Alloying anodes are likely to be a poor choice for KIBs, because the same issues that plague them in LIBs and NIBs are only exacerbated in KIBs (i.e., higher voltage, lower capacity, even higher volume increase upon alloying, all resulting in drastically reduced energy density, especially volumetric).<sup>[13]</sup> On the other hand, intercalation anodes have been shown to be stable for long term cycling, but suitable candidates with higher capacity and low voltage still need to be found. Finally, conversion anodes and organic anode materials are still in the very early stage of development, and should be further evaluated.

## 3. Cathode Materials

Potassium can be stored in a wide variety of structures: hexacyanometallates, oxides, polyanionic compounds, and organic materials. Although efforts to discover and develop new cathode materials for KIBs are in their infancy compared with those for anodes, several results reported to date demonstrate promising K-storage capability, and a rapid advancement of research in this area is expected. In this section, we review the ongoing research activity on cathode materials for KIBs, providing our key findings in four subsections on different material systems.

### 3.1. Hexacyanometallate Groups (Prussian Blue Analogues)

Hexacyanometallates, also known as Prussian blue analogues, with a nominal formula of  $K_xM_A[M_B(CN)_6]$  ( $0 \leq x \leq 2$ ) have an open framework to host K ions. **Figure 7a** presents a schematic illustration of a conventional unit cell of a hexacyanometallate with 1 K per formula unit ( $x = 1$ ).<sup>[81]</sup> A chain of  $M_A$ – $N \equiv C$ – $M_B$  arranged along the  $\langle 001 \rangle$  direction of the cubic unit cell generates alternating  $M_A N_6$  and  $M_B C_6$  octahedra, providing a large interstitial site for K ions surrounded by the cyanide ligands. For  $x = 1$ , the site is half filled. The structure allows for a 3D diffusion pathway, potentially leading to fast K intercalation. Thus, Prussian blue analogues are considered attractive candidates for KIB cathode materials.<sup>[18,19]</sup>

These materials are commonly synthesized by precipitation, with the K content ( $x$ ) ranging from 0 to 2 in  $K_xM_A[M_B(CN)_6]$ ; in addition, the  $M_A$  content can be tailored by selecting appropriate oxidation states of the  $M_A$  precursors. For example,  $KFe[Fe(CN)_6]$  is precipitated when  $FeCl_3$  is added to an aqueous  $K_4Fe(CN)_6$  solution,<sup>[82]</sup> and  $K_2Mn[Fe(CN)_6]$  is precipitated when  $Mn(NO_3)_2$  is added to an aqueous  $K_4Fe(CN)_6$  solution.<sup>[83]</sup> However, crystal water from the synthesis tends to be incorporated into the structure, replacing the entire  $[M_B(CN)_6]$  unit or occupying the interstitial site, as illustrated in **Figure 7b**,<sup>[81,84]</sup> leading to a composition that should be reported as  $K_xM_A[M_B(CN)_6]_{1-z} \cdot nH_2O$ . Although the water content varies with the synthesis protocols, complete dehydration in as-synthesized states is generally

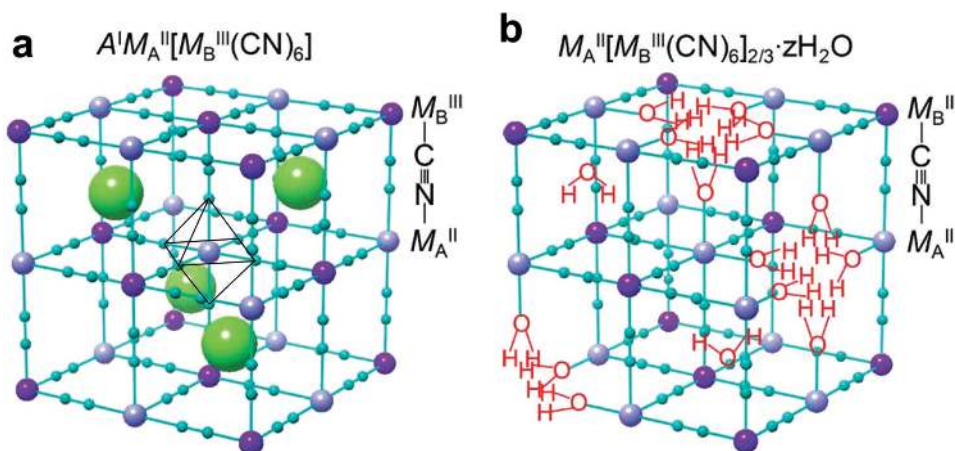


**Figure 7.** a,b) Schematic crystal structures of hexacyanometalate groups. Reproduced with permission.<sup>[81]</sup> Copyright 2011, Royal Society of Chemistry.

difficult because of the fast kinetics of the precipitation reaction.<sup>[85,86]</sup> Water incorporation lowers the amount of redox metal present in the structure and reduces the number of available sites for K ions, limiting the overall performance of the material.

Since the first demonstration of K-ion activity in  $KFe[Fe(CN)_6]$  with a nonaqueous electrolyte by Eftekhari in 2004,<sup>[87]</sup> for which  $\approx 1$  K reactivity was shown, several attempts have been made to explore the electrochemical properties of Prussian blue analogues.<sup>[82,83,88,89]</sup> Whereas the  $M_B$  site is generally occupied by Fe, the use of different transition metals for the  $M_A$  site leads to different K intercalation capacities and rate capability.<sup>[20]</sup> **Figure 8** presents voltage profiles of  $K_{1.75}Mn[Fe(CN)_6]_{0.93} \cdot 0.16H_2O$  as a function of specific capacity, as reported by Bie et al.<sup>[88]</sup> A reversible discharge capacity of  $137 \text{ mA h g}^{-1}$ , which reflects near theoretical K intercalation ( $1.88 \text{ K}$ ), is achieved at a cycling rate of  $30 \text{ mA g}^{-1}$ . Note that in the first few charge cycles, more than the theoretical capacity ( $\approx 155 \text{ mA h g}^{-1}$ ) was achieved, possibly due to parasitic reactions with the electrolyte and/or electrochemical dehydration, as often observed in Prussian blue analogues.<sup>[88]</sup> Two distinct plateaus were observed during charge (4.05 and 4.1 V) and discharge (3.85 and 4 V) with a small voltage step. Xue et al. suggested that the low-voltage plateau originates from a low-spin  $Fe^{2+/3+}$  redox reaction, whereas the high-voltage plateau reflects a high-spin  $Mn^{2+/3+}$  reaction.<sup>[83]</sup> These authors found voltage hysteresis between charge and discharge cycles and attributed it to electrolyte resistance due to the limited solubility of K salts in carbonate solvents. However, the authors did not provide specific evidence for these arguments, and the statement is at odds with the density functional theory prediction of faster mobility of K ion over Li and Na ions in nonaqueous electrolytes by Okoshi et al., and the experimental demonstration of this by Zhao et al. using electrochemical impedance spectroscopy.<sup>[27,90]</sup> Overall, the specific energy achievable in  $K_xMn[Fe(CN)_6]_{1-z} \cdot nH_2O$  with the two-electron redox reaction rivals that of  $LiFePO_4$ , though its volumetric energy density is unsatisfactory.<sup>[83,88]</sup> The full cell performance against the graphite anode shown in **Figure 8b** reveals excellent discharge rate capability, with delivery of  $62 \text{ mA h g}_{\text{cathode}}^{-1}$  at a  $2 \text{ A g}_{\text{cathode}}^{-1}$  rate.<sup>[88]</sup>

**Figure 9** shows voltage–capacity profiles of  $K_xM_A[Fe(CN)_6]_{1-z} \cdot nH_2O$  ( $M_A = Fe, Co, Ni, Cu$ ) in 2–4.5 V (vs  $K^+/K$ ) at room temperature. The reversible capacity achieved for the  $M_A = Fe$  composition is  $105 \text{ mA h g}^{-1}$ , whereas the other compositions deliver discharge capacities equal to or less than  $65 \text{ mA h g}^{-1}$ .<sup>[91]</sup> From **Figures 8** and **9**, one can conclude that promising performance can be achieved in compositions with Mn and Fe in the  $M_A$  site. This difference in performance may be due to indirect effects rather than to the specific properties of the redox center. Wu et al. observed that the overall water content increases as the atomic number of  $M_A$  increases, thereby affecting the electrochemical performance.<sup>[91]</sup>

The K intercalation mechanism can be studied using XRD. Bie et al. demonstrated how the structure of  $K_{1.75-x}Mn[Fe(CN)_6]_{0.93} \cdot 0.16H_2O$  evolves during electrochemical cycling.<sup>[88]</sup> Upon K extraction, the material undergoes a two-phase reaction from a structure with monoclinic (space group  $P2_1/n$ ) to a cubic (space group  $Fm-3m$ ) structure in the range  $0.4 < x < 0.9$ , which corresponds to the voltage plateau at 4.08 V in **Figure 8a**. Further potassium extraction transforms the cubic phase to a tetragonal (space group  $I-4m2$ ) phase through a two-phase reaction from  $x = 1.4$  to the end of charge. This reaction appears as a plateau at 4.11 V in **Figure 8a**. These authors suggested that the monoclinic-cubic transition is due to a transition from cooperatively rotated  $MnN_6$  and  $FeC_6$  polyhedra ( $K \approx 2$ ) to an unrotated alignment ( $K \approx 1$ ) as illustrated in **Figure 10**.<sup>[88]</sup> The cubic-to-tetragonal transition, on the other hand, can be explained by the Jahn–Teller distortion caused by the high-spin  $Mn^{3+}$ .<sup>[88]</sup> Note that when the  $M_A$  site is occupied by Jahn–Teller inactive elements such as high-spin  $Fe^{3+}$ , the cubic-to-tetragonal phase transformation is unobservable;<sup>[82,83]</sup> and instead a solid-solution type intercalation reaction occurs.

High specific energy and excellent cycling stability make Prussian blue analogues attractive cathode materials for K storage. In addition, the material uses earth-abundant Fe and Mn redox centers and is synthesizable by a scalable precipitation method, satisfying the low-cost requirement for development of large-scale ESSs. Still, there is room for improvement to achieve higher energy storage capacity. Given that the water

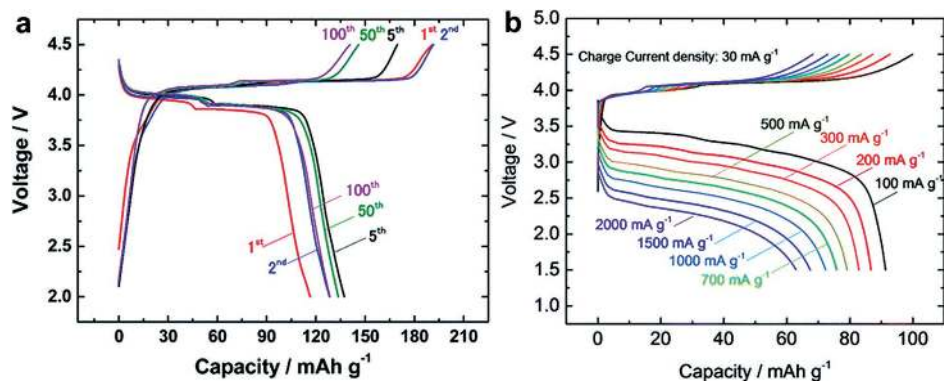


**Figure 8.** a) Typical charge/discharge profiles of  $K_{1.75}Mn[Fe(CN)_6]_{0.93} \cdot 0.16H_2O$  at  $30 \text{ mA g}_{\text{cathode}}^{-1}$ . b) Rate capability of KIB using  $K_{1.75}Mn[Fe(CN)_6]_{0.93} \cdot 0.16H_2O$  cathode and graphite anode. Reproduced with permission.<sup>[88]</sup> Copyright 2017, Royal Society of Chemistry.

content directly affects the electrochemical performance, synthesizing dehydrated composition will further enhance the specific energy effectively.

### 3.2. Layered Oxides

Layered transition metal oxides, used in LIBs and NIBs, are considered potential candidates for K storage materials. These materials generally have high theoretical energy density resulting from their close-packed structure.<sup>[92,93]</sup> As a result, the

most studied K-layered compounds have structures and transition metal content similar to those used in LIBs and NIBs.

Layered compounds can be conveniently categorized using an alphanumeric expression developed by Delmas et al.<sup>[94]</sup> In this notation, a letter describes the alkali metal sites as edge-sharing octahedral (O) or face-sharing prismatic (P) sites. The transition metals occupy the octahedral site in the next layer, framing alternating alkali and transition metal slabs. The number in the notation refers to the periodicity of the slab stacking. For instance, octahedral alkali metal and octahedral transition metal slabs repeat in a period of three

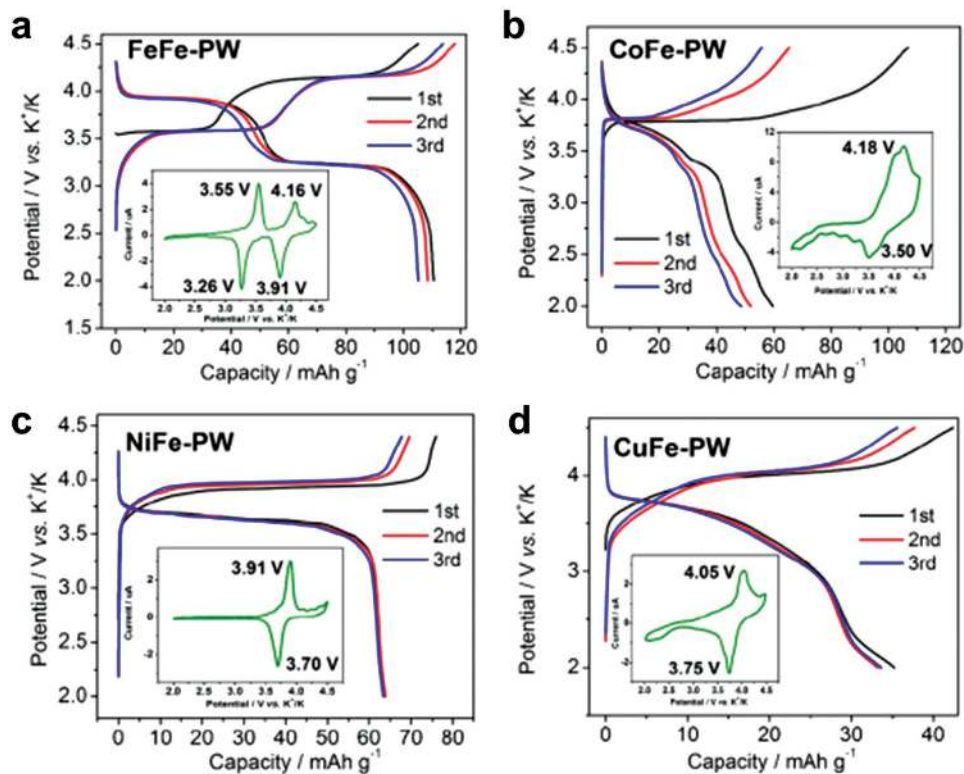


**Figure 9.** Charge/discharge profiles of a) FeFe-PW, b) CoFe-PW, c) NiFe-PW, and d) CuFe-PW where PW stands for Prussian white, one of the Prussian blue analogues with a nominal  $K_2M_4[Fe(CN)_6]$ . Reproduced with permission.<sup>[91]</sup> Copyright 2017, Elsevier.

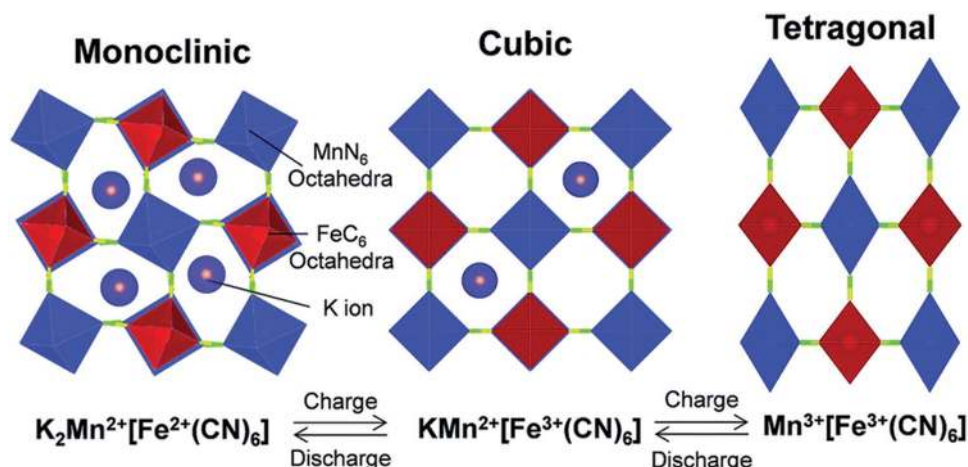


**Figure 10.** Crystal structures and phase transitions observed upon electrochemical potassium extraction (charging) and insertion (discharging). Reproduced with permission.<sup>[88]</sup> Copyright 2017, Royal Society of Chemistry.

(ABCABC stacking) in an O3-type layered structure, whereas prismatic alkali metal and octahedral transition metal slabs repeat in a period of two (ABBA stacking) in a P2-type layered structure or three (ABBCCA stacking) in a P3-type layered structure.<sup>[94]</sup>

Vaalma et al. demonstrated that a layered compound can be a host for K storage.<sup>[24]</sup> They evaluated  $K_{0.3}MnO_2$ , which forms in an orthorhombic distortion of the P2-type structure, (*Cmcm* space group) as a cathode for KIBs. The  $K_{0.3}MnO_2$  cathode delivered reversible capacities of  $\approx 70 \text{ mA h g}^{-1}$  in the voltage range of 1.5–3.5 V, as shown in **Figure 11a**, but exhibited poor cyclability in a more extended voltage range (1.5–4 V). These authors claimed that the large volume change and layer gliding upon K extraction are likely responsible for the capacity degradation but no direct evidence to substantiate that mechanism is available. The authors also demonstrated the practical feasibility of a rocking-chair KIB with a  $K_{0.3}MnO_2$  cathode and hard carbon anode (after prepotassiation). This full cell delivered a reversible discharge capacity of  $82 \text{ mA h g}^{-1}$  (based on the cathode).

Later, Wang et al. proposed  $K_{0.7}Mn_{0.5}Fe_{0.5}O_2$  nanowires as a cathode material for KIBs.<sup>[95]</sup> Although the XRD pattern of these nanowires is similar to that of a typical layered compound, the detailed structure could not be defined. The

nanowire was composed of 10–20 nm nanocrystallites with a 4.8 wt% carbon coating. The  $K_{0.7}Mn_{0.5}Fe_{0.5}O_2$  nanowire cathode provided a high specific capacity of  $\approx 180 \text{ mA h g}^{-1}$  with an average voltage of  $\approx 2.25 \text{ V}$  at  $20 \text{ mA g}^{-1}$  in the voltage range of 1.5–4.0 V (Figure 11b) and maintained  $\approx 70\%$  of its initial capacity after 45 cycles. The nanowire morphology resulted in superior specific capacity and rate capability compared to a nanoparticle morphology, a result the authors attribute to the interconnected nanostructure providing fast K kinetics. In situ XRD characterization revealed that depotassiation occurs via a two-phase reaction at a low state of charge and proceeds upon further charge with a solid-solution reaction. The discharge process follows the opposite reaction, indicating reversible K de/intercalation. The authors also demonstrated the practical feasibility of a  $K_{0.7}Mn_{0.5}Fe_{0.5}O_2$  cathode by constructing a full cell with a soft carbon anode, which delivered a reversible capacity of  $\approx 82 \text{ mA h g}^{-1}$  at  $40 \text{ mA g}^{-1}$  based on the cathode weight.

Recently, Hironaka et al.<sup>[58]</sup> and Kim et al.<sup>[57]</sup> reported P2-type  $K_xCoO_2$  ( $x \approx 0.4$  and  $0.6$ , respectively) cathodes for KIBs. According to Hironaka et al., P2-type  $K_{0.4}CoO_2$  exhibits a reversible capacity of  $\approx 60 \text{ mA h g}^{-1}$  between 2.0 and 3.9 V.<sup>[58]</sup> However, Kim et al. demonstrated that P2- $K_{0.6}CoO_2$  delivers a reversible capacity of  $\approx 80 \text{ mA h g}^{-1}$  between 1.7 and 4.0 V.<sup>[57]</sup> The different K activities can likely be attributed to different cut-off

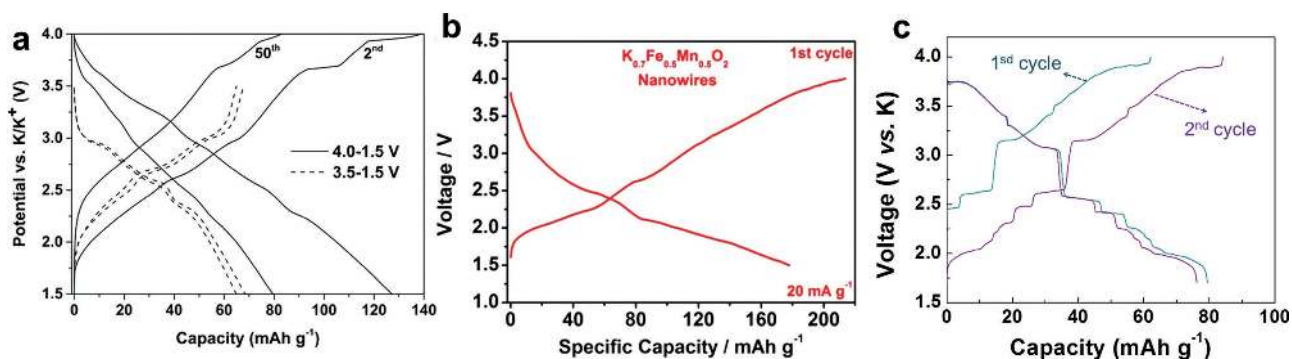


**Figure 11.** a) Galvanostatic measurements of  $K_{0.3}MnO_2$ . Reproduced with permission.<sup>[24]</sup> Copyright 2016, The Electrochemical Society. b) Galvanostatic measurements of  $K_{0.7}Fe_{0.5}Mn_{0.5}O_2$ . Reproduced with permission.<sup>[95]</sup> Copyright 2016 American Chemical Society. c) Galvanostatic measurements of  $K_{0.6}CoO_2$  cathode materials in K half-cell configurations. Reproduced with permission.<sup>[57]</sup> Copyright 2017, WILEY-VCH.

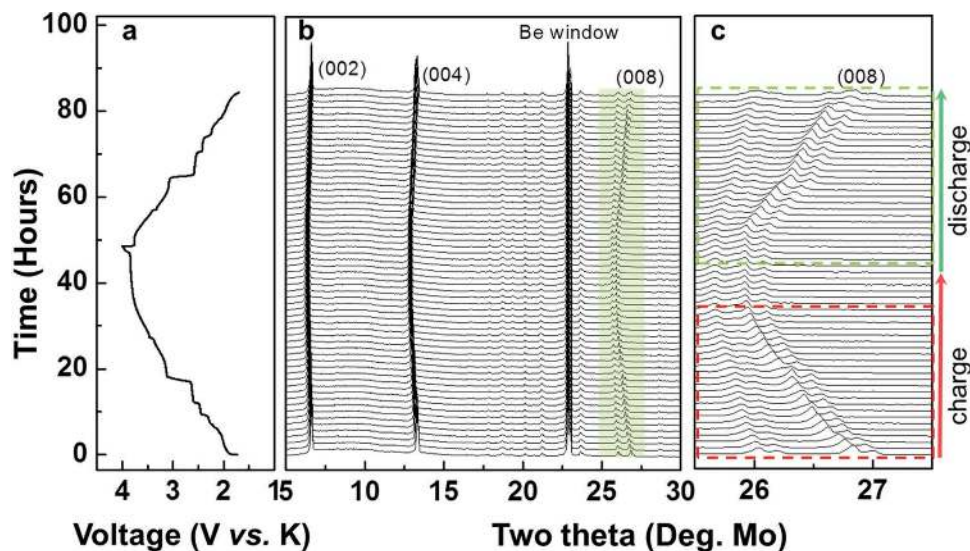


**Figure 12.** In situ XRD characterization of P2-type  $K_{0.6}CoO_2$  upon charge/discharge. a) Typical charge/discharge profiles of P2-type  $K_{0.6}CoO_2$  at a current rate of  $2\text{ mA g}^{-1}$ . b) In situ XRD patterns from  $15^\circ$  to  $30^\circ$ . c) (008) peaks obtained from in situ XRD. Reproduced with permission.<sup>[57]</sup> Copyright 2017, WILEY-VCH.

voltages. Figure 11c presents capacity–voltage curves of P2-type  $K_{0.6}CoO_2$ , which exhibit stair-like charge/discharge profiles, indicating multiple phase transitions upon K de/intercalation. In situ XRD (Figure 12) shows that upon charge, the (008) peak shifts to lower angles, indicative of *c*-axis expansion due to the increasing coulombic repulsion between the oxygen layers when K is extracted. In addition, asymmetric peak evolutions observed for the (008) peak suggest multiple phase transitions in  $K_xCoO_2$  even though the P2 framework is maintained. Hence, the phase transitions observed are likely due to  $K^+$ /vacancy ordering. Upon discharge, the (008) peak shifts back to its original position, confirming the reversibility of K extraction and insertion. Kim et al. also demonstrated the practical feasibility of a P2-type  $K_{0.6}CoO_2$  by pairing with a graphite anode in a full cell, delivering a reversible capacity of  $\approx 53\text{ mA h per g}$  of cathode.<sup>[57]</sup>

In general, the voltage curves of K layered compounds have steeper slopes than those of Li and Na systems. This feature is likely attributable to the size of  $K^+$ : The  $K^+$  creates a much larger slab spacing in  $K_xMO_2$  compounds compared to the  $Na_xMO_2$  and  $Li_xMO_2$  analogues. The larger oxygen–oxygen distance leads to less effective screening of the  $K^+K^+$  repulsion, creating large effective ordering interactions. As a result, a remarkable amount of stable intermediate phases is stabilized showing up as a multitude of features in the voltage curve upon K de/intercalation. The larger average slope in the voltage curves, in turn, results in a reduced capacity for a given voltage window. In practice, this behavior leads to a low specific capacity of K layered compounds, and is a considerable drawback for layered  $K_xMO_2$  compounds as compared to their Na and Li analogues.

### 3.3. Polyanionic Compounds

Polyanionic compounds are promising cathode materials because of their high stability against oxygen loss and

the ability to tune the redox voltage through the inductive effect.<sup>[96–98]</sup> In addition, polyanionic frameworks are expected to better screen the K–K repulsion in the structure, unlike the layered structure where the strong K–K repulsion limits the K storage capability.<sup>[57]</sup> In this respect, polyanion materials may be particularly relevant for KIBs.

Recham et al. demonstrated that fluorosulfates can reversibly intercalate Li, Na, and K.<sup>[99]</sup> They prepared  $FeSO_4F$ , consisting of chains of  $FeO_4F_2$  octahedra linked through F atoms, by electrochemically extracting K from  $KFeSO_4F$  using Li/ $KFeSO_4F$  cells, and evaluated the electrochemical properties for each alkali metal. As observed in Figure 13a–c,  $FeSO_4F$  can accommodate  $\approx 0.9$  Li,  $\approx 0.85$  Na, and  $\approx 0.8$  K. Interestingly, the voltage steps in the K cells are the most pronounced, implying the presence of multiple stable intermediate phases. In addition, Fedotov et al. developed  $KVPO_4F$ , which has a similar structure as  $KFeSO_4F$ , and extracted  $\approx 0.85$  K from  $KVPO_4F$  in order to use the material as a charged cathode for LIBs.<sup>[100]</sup> Very recently, Chihara et al. reported that  $KVPO_4F$  can also be used for KIBs,<sup>[101]</sup> delivering  $\approx 90\text{ mA h g}^{-1}$  with an average voltage of  $\approx 4.13\text{ V}$ , which is significantly higher than the voltages observed for K layered compounds.

Amorphous  $FePO_4$  was reported as a host material for various cations, including Li, Na, K, Mg, and Zn, by Mathew et al.<sup>[102]</sup> These researchers argued that the amorphous structure with short-range ordering can facilitate guest-ion insertions regardless of their sizes. Amorphous  $FePO_4$  was shown to reversibly insert K up to  $\approx 150\text{ mA h g}^{-1}$  with an average voltage of  $\approx 2.5\text{ V}$  (Figure 13d). Interestingly, their ex situ XRD results reveal an electrochemically induced amorphous-to-crystalline transition, as shown in Figure 13e. Upon K insertion, a new XRD pattern evolved, which corresponds to  $KFe_2(PO_4)_2$ ; upon subsequent K extraction, all the XRD peaks disappear, indicating the formation of an amorphous phase. Recently, the use of  $K_3V_2(PO_4)_3$  as a cathode for KIBs was proposed by Han et al.<sup>[103]</sup> Although the stoichiometry might suggest

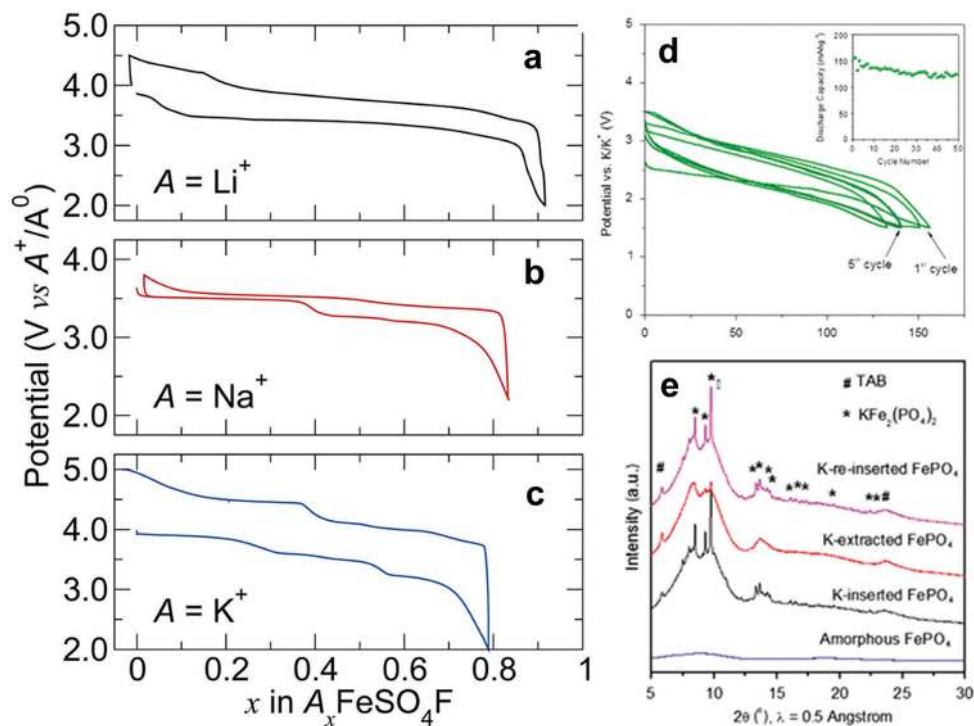


**Figure 13.** Typical charge/discharge profiles of  $\text{FeSO}_4\text{F}$  in a) Li, b) Na, and c) K half cells. Reproduced with permission.<sup>[99]</sup> Copyright 2012, American Chemical Society. d) Capacity–voltage curve of amorphous  $\text{FePO}_4/\text{K}$  cells. e) Ex situ XRD characterization of amorphous  $\text{FePO}_4$ . Reproduced with permission.<sup>[102]</sup> Copyright 2014, Nature Publishing Group.

a NASICON-type compound, the detailed crystal structure of  $\text{K}_3\text{V}_2(\text{PO}_4)_3$  has not been identified. The  $\text{K}_3\text{V}_2(\text{PO}_4)_3$  cathode delivered a reversible capacity of  $\approx 54 \text{ mA h g}^{-1}$  with an average voltage of  $\approx 3.7 \text{ V}$  and retained  $\approx 80\%$  of the initial capacity after 100 cycles.

Polyanionic compounds can be good candidates because of their high working voltage.  $\text{KVPO}_4\text{F}$  especially provides the highest working voltage ( $\approx 4.13 \text{ V}$  versus  $\text{K}/\text{K}^+$ ) among cathode materials developed to date. In addition, the wide pool of polyanion species, including  $(\text{PO}_4)^{3-}$ ,  $(\text{SO}_4)^{2-}$ , and  $(\text{P}_2\text{O}_7)^{4-}$  can provide many opportunities to find new crystal structures for K storage.

### 3.4. Organic Cathodes

Xing et al. observed electrochemical activity for K storage in organic compounds, in which the charge transfer occurs in  $\text{C}=\text{O}$  bonds, and an aromatic ring hosts the K ions.<sup>[104,105]</sup> Using 3,4,9,10-perylene-tetracarboxylic acid-dianhydride as a K storage host, they reported a capacity of  $129 \text{ mA h g}^{-1}$  for the first discharge at  $20 \text{ mA g}^{-1}$  in the voltage range of 1.2–3.2 V with  $0.8 \text{ M KPF}_6$  in EC:DEC with a 1:1 ratio by volume.<sup>[104]</sup> However, ex situ XRD and infrared spectroscopy indicate that the structural evolution upon K insertion and extraction is irreversible, suggesting possible parasitic contributions to the capacity. K storage in poly(anthraquinonyl) sulfide (PAQS) was also demonstrated by Jian et al.<sup>[105]</sup> One PAQS molecule was observed to uptake two K ions upon discharge ( $211 \text{ mA h g}^{-1}$  at  $20 \text{ mA g}^{-1}$  in 1.5–3.4 V) when using  $0.5 \text{ M KTFSI}$  in mixed

dimethoxyethane and dioxolane solution (1:1 ratio by volume). Zhao et al. showed that oxocarbon ( $\text{C}_6\text{O}_6$ ) can cycle two K ions in the voltage range of 1–3.2 V, delivering a capacity of  $212 \text{ mA h g}^{-1}$  at  $0.2 \text{ C}$ .<sup>[90]</sup> These authors also compared the kinetics of K storage in the oxocarbon with that for Li and Na and found that the K diffusivity estimated by cyclic voltammetry is higher than those of Li and Na for the same system. Overall, the energy densities of organic cathode compounds are low because of the large molecular volume combined with a low operating voltage. In addition, the underlying mechanisms for K storage in organic materials are not yet clear: further investigation is needed to ensure whether reversible redox reaction occurs in the solid phase or by dissolution reprecipitation in the electrolyte, as discussed in other alkali metal systems.<sup>[106]</sup> Nevertheless, some materials exhibit higher rate capability than their Li or Na counterparts and reasonable reversibility, suggesting opportunities for low-cost, high-power applications for these materials.

## 4. Discussion and Outlook

Several types of anode materials have already been proposed for KIBs, closely resembling those reported for LIBs and NIBs. The majority of these candidates are carbonaceous materials. Graphite, in particular, has been demonstrated to be viable and to exhibit remarkable rate capabilities by Komaba et al.<sup>[26]</sup> Subsequent studies confirmed that graphite has low migration barriers for K diffusion, high capacity, and sufficiently low intercalation potential, making it truly promising for KIBs;



however, a stable SEI is key to obtaining good performance upon repeated cycling. Therefore, suitable binders (such as PANa) and electrolytes (such as EC:PC or EC:DEC with KPF<sub>6</sub> or KTFSI salts) must be used. When these measures are taken, the performance of graphite anodes in KIBs can reach levels comparable to those in LIBs with the additional potential benefit of a superior charge-rate capability because of the higher potassiation voltage. Although several other carbons such as soft and hard carbon, composites, or graphene-related (possibly doped) materials have been demonstrated to perform well in KIBs, they nevertheless lead to low volumetric densities and often have higher voltage than graphite, which will negatively affect the overall energy density of the cell. These drawbacks have been well documented for NIBs, for which graphite anodes cannot be used.

Among noncarbonaceous anodes, few possibilities among those reported to date are truly promising. Anodes based on alloying reactions are unlikely to be good candidates: the capacities and voltages are calculated to be lower and higher, respectively, than those of LIBs and NIBs, resulting in lower energy densities. Moreover, the problem of avoiding large volume expansion upon alloying, which already plagues Li and Na, is exacerbated for K, making long-term cycling difficult to achieve.

Intercalation anodes are potential alternatives to carbon-based ones: titanium-containing materials such as K<sub>2</sub>Ti<sub>8</sub>O<sub>17</sub> can reach rather high capacities of 181.5 mA h g<sup>-1</sup> at 20 mA g<sup>-1</sup>. Unfortunately, their voltages are quite high; therefore, if better candidates with lower voltages (and possibly higher density) can be found, these materials could be used in full KIB cells. However, it should be stressed that more than 20 years of research to find titanates with voltages lower than that of Li<sub>4</sub>Ti<sub>5</sub>O<sub>12</sub> delivered no significant results.

Finally, organic anodes using K<sub>2</sub>TP and K<sub>2</sub>PC with remarkable capacities that are stable for more than 100 cycles have also been reported. Their drawback is the low volumetric energy density of organic molecules; however, because organic cathodes have also been reported, a full-organic KIB is a practical possibility. As with all small molecular organic species, solubility of the charged and/or discharged state in the organic electrolyte solvent upon prolonged cycling should be carefully investigated.

In KIBs, the development of cathode materials that can deliver high gravimetric and volumetric energy density comparable to those of LIBs and NIBs is crucial. Even though applications such as grid do not fundamentally require high energy density, a lower energy density of cells often leads to higher cost per kWh simply because more cells have to be used. **Figure 14** plots the gravimetric and volumetric energies of cathode materials for KIBs reported to date. Overall, the gravimetric energies are comparable to those of NIB cathode materials. Among the cathodes, the Prussian blue analogues provide the highest gravimetric energies; however, they exhibit less volumetric energy than the layered compounds because of their low density. Layered K<sub>0.7</sub>Fe<sub>0.5</sub>Mn<sub>0.5</sub>O<sub>2</sub> provides the highest volumetric energy, comparable to that of Na<sub>0.74</sub>CoO<sub>2</sub>. It is notable that even though the research on KIBs has just begun, some positive electrodes already exhibit good performance, comparable to that of NIB technology, leading to their demonstration in practical rocking-chair KIBs.<sup>[24,57,88,95,101]</sup> Nevertheless, more

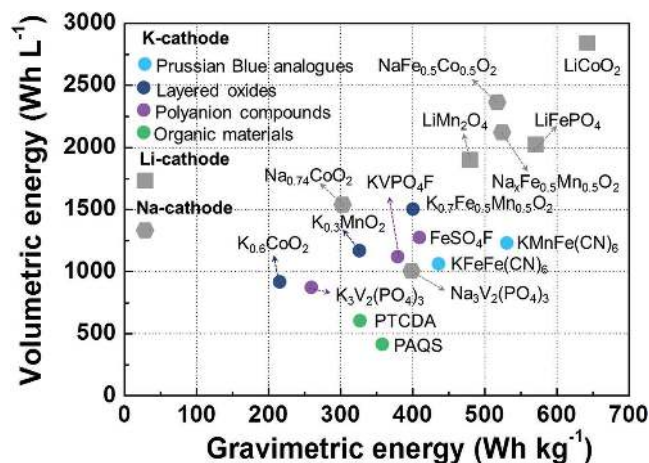


**Figure 14.** Demonstrated, gravimetric versus volumetric energy of cathode materials for KIBs and comparison with Li and Na cathode materials. The mass and volume of the active electrode materials were considered to calculate the gravimetric and volumetric energies. The data were obtained from the literature.<sup>[24,57,88,95,99,101,104,107]</sup>

focused research on cathode materials should be conducted for such a nascent chemistry to become practical.

To provide further guidelines for the investigation of cathode materials for KIBs, we predicted the K-intercalation voltages of various cathode materials using DFT/generalized gradient approximation (GGA) with Hubbard U correction (GGA+U)<sup>[108]</sup> and Equation (1). The U values of 3.5 eV, 3.9 eV, 4.0 eV, and 3.4 eV were used for Cr, Mn, Fe, and Co, respectively.<sup>[109]</sup>

**Figure 15a** presents the calculated average voltages of layered P2- and P3-K<sub>x</sub>MO<sub>2</sub> (0 ≤ x ≤ 0.66, M = Cr, Mn, Co) for Na and K insertion. In all cases, the average K and Na-insertion voltages are similar. Nevertheless, the larger voltage slope that has been observed for K-insertion leads to a lower specific capacity and presents a fundamental limitation for K-layered cathodes. In addition, the K layered compounds developed to date all have K-deficient compositions (x < 0.7 in K<sub>x</sub>MO<sub>2</sub>). Because the alkali ions in a full cell tend to originate from the cathode materials, it is critical to develop fully potassiated K layered compounds (KMO<sub>2</sub>).

We also calculated the average voltages of A<sub>x</sub>FePO<sub>4</sub> (A = Li, Na, K) and A<sub>x</sub>FeSO<sub>4</sub>F (A = Li, Na, K) at 0 ≤ x ≤ 1, as shown in **Figure 15b**. For each compound, voltages were first calculated in the preferred structure for the composition, namely, LiFePO<sub>4</sub> (Pnma), maricite NaFePO<sub>4</sub> (Pnma), KFePO<sub>4</sub> (P2<sub>1</sub>/n), tavorite LiFeSO<sub>4</sub>F (P-1), NaFeSO<sub>4</sub>F (C2/c), and KFeSO<sub>4</sub>F (C2/c). In this comparison, the K-compounds exhibit slightly higher average voltages than their Na analogues and comparable voltages to their Li analogues. To study the relation between the voltage and structural preferences for Li, Na, and K compounds, we also compared the K, Na, and Li average voltages across a fixed structure namely the olivine structure of LiFePO<sub>4</sub> and the KFeSO<sub>4</sub>F structure. We fully relaxed each structure with Li, Na, and K ions using DFT and calculated their average voltages. Because the K<sup>+</sup> ionic radius (138 pm) is much larger than that of Li<sup>+</sup> (76 pm) and Na<sup>+</sup> (102 pm), the K insertion into olivine Li<sub>x</sub>FePO<sub>4</sub> (x = 0) structure is less favorable than either Na or Li insertion, resulting in lower K insertion voltage as observed in **Figure 15b**. By

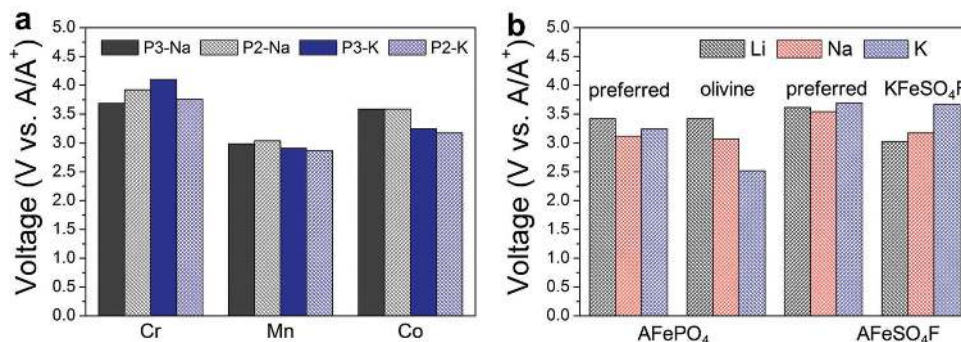


**Figure 15.** Calculated average voltages of a) layered P2- and P3-A<sub>x</sub>MO<sub>2</sub> ( $0 \leq x \leq 0.66$ , A = Na, K; M = Cr, Mn, Co) and b) AFePO<sub>4</sub> and AFeSO<sub>4</sub>F (A = Li, Na, K). For each composition two structures were considered. The first structure is the thermodynamically preferred structure for each alkali metal as listed in the Inorganic Crystal Structure Database (ICSD). To compare the voltages for different alkali metals within the same framework, the voltages for AFePO<sub>4</sub> were also calculated within a common structure: olivine LiFePO<sub>4</sub> for AFePO<sub>4</sub> and KFeSO<sub>4</sub>F for AFeSO<sub>4</sub>F.

contrast, the voltage of AFeSO<sub>4</sub>F (A = Li, Na, K) within the KFeSO<sub>4</sub>F framework increases with increasing ionic size due to the large cavities for alkali ions in the KFeSO<sub>4</sub>F framework. These results imply that K compounds exhibit stronger structural preferences than Na compounds because of their larger ionic radii.

The comparable voltages of K compounds and their Na analogues can be explained in terms of the cathodic and anodic contributions to the redox potential. The anodic contribution is determined by the energy cost for extracting an alkali atom from the metal anode. The smaller cohesive energy of K metal (0.934 eV per atom) compared with those of Na metal (1.113 eV per atom) and Li metal (1.63 eV per atom) implies a smaller energy cost for K extraction than for Li and Na extraction, increasing the voltages of K compounds. The cathodic contribution is determined by the energy gain for alkali-ion insertion into a host structure. The formation energy of K<sub>2</sub>O (−363 kJ mol<sup>−1</sup>) is lower than those of Na<sub>2</sub>O (−417.98 kJ mol<sup>−1</sup>) and Li<sub>2</sub>O (−598.73 kJ mol<sup>−1</sup>), implying that K–O bonding is generally weaker than Na–O and Li–O bonding. Thus, the energy gain for K insertion is lower than that for Na or Li insertion, decreasing the voltages of K compounds. However, the difference in the formation energy between K<sub>2</sub>O and Na<sub>2</sub>O is much less than that between K<sub>2</sub>O and Li<sub>2</sub>O. The negative cathodic contribution can be compensated by a positive anodic contribution; thus, K cathode compounds have redox potentials that are comparable to those of Na cathode compounds.

## 5. Summary

In this review, we summarized the most up-to-date progress in materials development for K-ion batteries and discussed some of the challenges and opportunities. One of the greatest advantages motivating KIBs and differentiating them from NIBs is the K intercalation into graphite anodes, though its reversibility requires careful tuning of binders and electrolytes. Among other possible anode chemistries, alloying anodes are hardly good candidates: they exhibit substantial capacity but have high voltages and suffer from large volume expansion. These issues could be moderated by particle nanosizing or morphology optimization. By contrast, intercalation anodes exhibit small

volume change and good capacity retention, but so far have shown limited capacity. We also reviewed a wide variety of cathode chemistries. The K layered oxides may not be as attractive as in the Li and Na systems as the large K size only allows a limited amount of K into the structure, thereby reducing the achievable capacity. We suggest that there may be more opportunities in polyanionic materials or Prussian blue analogues that have multielectron redox reactions.

## Acknowledgements

H.K., J.C.K., and M.B. contributed equally to this work. This work was supported by the Laboratory Directed Research and Development Program of Lawrence Berkeley National Laboratory under the U.S. Department of Energy (Contract No. DE-AC02-05CH11231). This work used the Extreme Science and Engineering Discovery Environment (XSEDE), which is supported by National Science Foundation Grant No. ACI-1053575, and resources of the National Energy Research Scientific Computing Center (NERSC), a DOE Office of Science User Facility supported by the Office of Science of the U.S. Department of Energy under Contract No. DE-AC02-05CH11231. H.K.'s contribution was also supported by the Basic Science Research Program through the National Research Foundation of Korea (NRF) funded by the Ministry of Education (2017R1A6A3A03001850). This article was published as part of the *Advanced Energy Materials* Excellence in Energy special series.

## Conflict of Interest

The authors declare no conflict of interest.

## Keywords

batteries, electrodes, K-ion, next-generation, potassium

Received: August 29, 2017  
 Revised: September 19, 2017  
 Published online:

[1] L. Doman, EIA projects 48% increase in world energy consumption by 2040, U.S. Energy Information Administration,

- <https://www.eia.gov/todayinenergy/detail.php?id=26212> (accessed: May 2017).
- [2] K. Kang, Y. S. Meng, J. Breger, C. P. Grey, G. Ceder, *Science* **2006**, *311*, 977.
  - [3] Energy Storage for Power Systems Applications: A Regional Assessment for the Northwest Power Pool (NWPP), Pacific Northwest National Laboratory, [http://www.pnl.gov/main/publications/external/technical\\_reports/PNNL-19300.pdf](http://www.pnl.gov/main/publications/external/technical_reports/PNNL-19300.pdf) (accessed: May 2017).
  - [4] G. Ceder, Y. M. Chiang, D. R. Sadoway, M. K. Aydinol, Y. I. Jang, B. Huang, *Nature* **1998**, *392*, 694.
  - [5] K. C. Divya, J. Østergaard, *Electr. Power Syst. Res.* **2009**, *79*, 511.
  - [6] H. Kim, H. Kim, Z. Ding, M. H. Lee, K. Lim, G. Yoon, K. Kang, *Adv. Energy Mater.* **2016**, *6*, 1600943.
  - [7] H. Vikström, S. Davidsson, M. Höök, *Appl. Energy* **2013**, *110*, 252.
  - [8] P. W. Gruber, P. A. Medina, G. A. Keoleian, S. E. Kesler, M. P. Everson, T. J. Wallington, *J. Ind. Ecol.* **2011**, *15*, 760.
  - [9] J. Heyd, G. E. Scuseria, M. Ernzerhof, *J. Chem. Phys.* **2006**, *124*, 219906.
  - [10] M. K. Aydinol, A. F. Kohan, G. Ceder, *J. Power Sources* **1997**, *68*, 664.
  - [11] E. A. Olivetti, G. Ceder, G. G. Gaustad, X. Fu, *Joule* **2017**, *1*, 229.
  - [12] S.-W. Kim, D.-H. Seo, X. Ma, G. Ceder, K. Kang, *Adv. Energy Mater.* **2012**, *2*, 710.
  - [13] V. L. Chevrier, G. Ceder, *J. Electrochem. Soc.* **2011**, *158*, A1011.
  - [14] V. Palomares, P. Serras, I. Villaluenga, K. B. Hueso, J. Carretero-Gonzalez, T. Rojo, *Energy Environ. Sci.* **2012**, *5*, 5884.
  - [15] D. A. Stevens, J. R. Dahn, *J. Electrochem. Soc.* **2000**, *147*, 1271.
  - [16] H. Kim, J. Hong, Y.-U. Park, J. Kim, I. Hwang, K. Kang, *Adv. Funct. Mater.* **2015**, *25*, 534.
  - [17] H. Kim, J. Hong, G. Yoon, H. Kim, K.-Y. Park, M.-S. Park, W.-S. Yoon, K. Kang, *Energy Environ. Sci.* **2015**, *8*, 2963.
  - [18] A. Eftekhari, Z. Jian, X. Ji, *ACS Appl. Mater. Interfaces* **2017**, *9*, 4404.
  - [19] J. C. Pramudita, D. Sehwat, D. Goonetilleke, N. Sharma, *Adv. Energy Mater.*, **2017**, <http://doi.org/10.1002/aenm.201602911>.
  - [20] X. Wu, D. P. Leonard, X. Ji, *Chem. Mater.* **2017**, *29*, 5031.
  - [21] Abundance in Earth's Crust of the elements, <http://periodictable.com/Properties/A/CrustAbundance.html> (accessed: May 2017).
  - [22] Abundance in the Ocean of the elements, <http://periodictable.com/Properties/A/OceanAbundance.html> (accessed: May 2017).
  - [23] U.S. Geological Survey, Mineral Commodities Summaries (2015), <https://pubs.er.usgs.gov/publication/70140094> (accessed: May 2017).
  - [24] C. Vaalma, G. A. Giffin, D. Buchholz, S. Passerini, *J. Electrochem. Soc.* **2016**, *163*, A1295.
  - [25] Y. Marcus, in *Pure and Applied Chemistry*, IUPAC, NC Vol. 57, **1985**, p. 1129.
  - [26] S. Komaba, T. Hasegawa, M. Dahbi, K. Kubota, *Electrochem. Commun.* **2015**, *60*, 172.
  - [27] M. Okoshi, Y. Yamada, S. Komaba, A. Yamada, H. Nakai, *J. Electrochem. Soc.* **2017**, *164*, A54.
  - [28] J.-M. Tarascon, *Nat. Chem.* **2010**, *2*, 510.
  - [29] S. P. ATACAMA, *The Economist*, <https://www.economist.com/news/business/21688386-amid-surge-demand-rechargeable-batteries-companies-are-scrambling-supplies> (accessed: May 2016).
  - [30] N. Yabuuchi, K. Kubota, M. Dahbi, S. Komaba, *Chem. Rev.* **2014**, *114*, 11636.
  - [31] W. Rüdorff, E. Schulze, *Z. Anorg. Allg. Chem.* **1954**, *277*, 156.
  - [32] D. E. Nixon, G. S. Parry, *J. Phys. D: Appl. Phys.* **1968**, *1*, 291.
  - [33] M. S. Dresselhaus, in *Festkörperprobleme 25: 5th General Conference of the Condensed Matter Division (CMD)* (Ed: P. Grosse), Springer, Berlin **1985**, p. 21; <https://doi.org/10.1007/BFb0108123>.
  - [34] Z. Wang, S. M. Selbach, T. Grande, *RSC Adv.* **2014**, *4*, 4069.
  - [35] Z. Jian, W. Luo, X. Ji, *J. Am. Chem. Soc.* **2015**, *137*, 11566.
  - [36] J. Zhao, X. X. Zou, Y. J. Zhu, Y. H. Xu, C. S. Wang, *Adv. Funct. Mater.* **2016**, *26*, 8103.
  - [37] Z. M. Xu, X. J. Lv, J. G. Chen, L. X. Jiang, Y. Q. Lai, J. Li, *Carbon* **2016**, *107*, 885.
  - [38] S. Thinius, M. M. Islam, P. Heitjans, T. Bredow, *J. Phys. Chem. C* **2014**, *118*, 2273.
  - [39] K. Persson, Y. Hinuma, Y. S. Meng, A. Van der Ven, G. Ceder, *Phys. Rev. B* **2010**, *82*, 125416.
  - [40] E. Irisarri, A. Ponrouch, M. R. Palacin, *J. Electrochem. Soc.* **2015**, *162*, A2476.
  - [41] Z. L. Jian, Z. Y. Xing, C. Bommier, Z. F. Li, X. L. Ji, *Adv. Energy Mater.* **2016**, *6*, 1501874.
  - [42] Z. Jian, S. Hwang, Z. Li, A. S. Hernandez, X. Wang, Z. Xing, D. Su, X. Ji, *Adv. Funct. Mater.*, **2017**, *27*, 1700324.
  - [43] C. Chen, Z. Chen, B. Zhang, L. Miao, J. Cai, L. Peng, Y. Huang, J. Jiang, Y. Huang, L. Zhang, J. Xie, *Energy Storage Materials* **2017**, *8*, 161.
  - [44] Z. Tai, Y. Liu, Q. Zhang, T. Zhou, Z. Guo, H. K. Liu, S. X. Dou, *Green Energy Environ.*, **2017**, *2*, 728.
  - [45] Y. Li, R. A. Adams, A. Arora, V. G. Pol, A. M. Levine, R. J. Lee, K. Akato, A. K. Naskar, M. P. Paranthaman, *J. Electrochem. Soc.* **2017**, *164*, A1234.
  - [46] Z. Xing, Y. Qi, Z. Jian, X. Ji, *ACS Appl. Mater. Interfaces* **2017**, *9*, 4343.
  - [47] W. Luo, J. Wan, B. Ozdemir, W. Bao, Y. Chen, J. Dai, H. Lin, Y. Xu, F. Gu, V. Barone, L. Hu, *Nano Lett.* **2015**, *15*, 7671.
  - [48] Z. C. Ju, S. Zhang, Z. Xing, Q. C. Zhuang, Y. H. Qiang, Y. T. Qian, *ACS Appl. Mater. Interfaces* **2016**, *8*, 20682.
  - [49] K. Share, A. P. Cohn, R. E. Carter, C. L. Pint, *Nanoscale* **2016**, *8*, 16435.
  - [50] K. Share, A. P. Cohn, R. Carter, B. Rogers, C. L. Pint, *ACS Nano* **2016**, *10*, 9738.
  - [51] G. Ma, K. Huang, J.-S. Ma, Z. Ju, Z. Xing, Q.-c. Zhuang, *J. Mater. Chem. A* **2017**, *5*, 7854.
  - [52] R. A. Adams, J.-M. Syu, Y. Zhao, C.-T. Lo, A. Varma, V. G. Pol, *ACS Appl. Mater. Interfaces* **2017**, *9*, 17872.
  - [53] A. P. Cohn, N. Muralidharan, R. Carter, K. Share, L. Oakes, C. L. Pint, *J. Mater. Chem. A* **2016**, *4*, 14954.
  - [54] H. Kim, G. Yoon, K. Lim, K. Kang, *Chem. Commun.* **2016**, *52*, 12618.
  - [55] R. A. ACS Applied Materials & Interfaces Huggins, *J. Power Sources* **1999**, *81–82*, 13.
  - [56] M. N. Obrovac, V. L. Chevrier, *Chem. Rev.* **2014**, *114*, 11444.
  - [57] H. Kim, J. C. Kim, S.-H. Bo, T. Shi, D.-H. Kwon, G. Ceder, *Adv. Energy Mater.* **2017**, *7*, 1700098.
  - [58] Y. Hironaka, K. Kubota, S. Komaba, *Chem. Commun.* **2017**, *53*, 3693.
  - [59] T. B. Massalski, H. Okamoto, P. Subramanian, L. Kacprzak, W. W. Scott, *Binary Alloy Phase Diagrams*, American Society for Metals, Metals Park, OH **1986**.
  - [60] W. D. McCulloch, X. Ren, M. Yu, Z. Huang, Y. Wu, *ACS Appl. Mater. Interfaces* **2015**, *7*, 26158.
  - [61] I. Sultana, T. Ramireddy, M. M. Rahman, Y. Chen, A. M. Glushenkov, *Chem. Commun.* **2016**, *52*, 9279.
  - [62] W. Zhang, J. Mao, S. Li, Z. Chen, Z. Guo, *J. Am. Chem. Soc.* **2017**, *139*, 3316.
  - [63] K. Zaghbi, M. Simoneau, M. Armand, M. Gauthier, *J. Power Sources* **1999**, *81–82*, 300.
  - [64] P. Senguttuvan, G. Rousse, V. Seznec, J. M. Tarascon, M. R. Palacin, *Chem. Mater.* **2011**, *23*, 4109.
  - [65] B. Kishore, G. Venkatesh, N. Munichandraiah, *J. Electrochem. Soc.* **2016**, *163*, A2551.
  - [66] J. Han, M. Xu, Y. Niu, G.-N. Li, M. Wang, Y. Zhang, M. Jia, C. m. Li, *Chem. Commun.* **2016**, *52*, 11274.

- [67] P. Senguttuvan, G. Rousse, M. E. Arroyo y de Dompablo, H. Vezin, J. M. Tarascon, M. R. Palacín, *J. Am. Chem. Soc.* **2013**, *135*, 3897.
- [68] J. Han, Y. Niu, S.-j. Bao, Y.-N. Yu, S.-Y. Lu, M. Xu, *Chem. Commun.* **2016**, *52*, 11661.
- [69] J. A. Woollam, R. B. Somoano, *Mater. Sci. Eng.* **1977**, *31*, 289.
- [70] X. Ren, Q. Zhao, W. D. McCulloch, Y. Wu, *Nano Res.* **2017**, *10*, 1313.
- [71] M. A. Py, R. R. Haering, *Can. J. Phys.* **1983**, *61*, 76.
- [72] Q. Deng, J. Pei, C. Fan, J. Ma, B. Cao, C. Li, Y. Jin, L. Wang, J. Li, *Nano Energy* **2017**, *33*, 350.
- [73] K. Lei, F. Li, C. Mu, J. Wang, Q. Zhao, C. Chen, J. Chen, *Energy Environ. Sci.* **2017**, *10*, 552.
- [74] M. Armand, S. Grugeon, H. Vezin, S. Laruelle, P. Ribiere, P. Poizot, J. M. Tarascon, *Nat. Mater.* **2009**, *8*, 120.
- [75] Y. Park, D.-S. Shin, S. H. Woo, N. S. Choi, K. H. Shin, S. M. Oh, K. T. Lee, S. Y. Hong, *Adv. Mater.* **2012**, *24*, 3562.
- [76] H. H. Lee, Y. Park, K.-H. Shin, K. T. Lee, S. Y. Hong, *ACS Appl. Mater. Interfaces* **2014**, *6*, 19118.
- [77] Y. Liang, Z. Tao, J. Chen, *Adv. Energy Mater.* **2012**, *2*, 742.
- [78] Y. Li, H. Zhan, L. Kong, C. Zhan, Y. Zhou, *Electrochem. Commun.* **2007**, *9*, 1217.
- [79] J. Cabana, L. Monconduit, D. Larcher, M. R. Palacín, *Adv. Mater.* **2010**, *22*, E170.
- [80] I. Sultana, M. M. Rahman, S. Mateti, V. G. Ahmadabadi, A. M. Glushenkov, Y. Chen, *Nanoscale* **2017**, *9*, 3646.
- [81] H. Tokoro, S.-i. Ohkoshi, *Dalton Trans.* **2011**, *40*, 6825.
- [82] C. Zhang, Y. Xu, M. Zhou, L. Liang, H. Dong, M. Wu, Y. Yang, Y. Lei, *Adv. Funct. Mater.* **2017**, *27*, 1604307.
- [83] L. Xue, Y. Li, H. Gao, W. Zhou, X. Lü, W. Kaveevivitchai, A. Manthiram, J. B. Goodenough, *J. Am. Chem. Soc.* **2017**, *139*, 2164.
- [84] F. Herren, P. Fischer, A. Ludi, W. Haelg, *Inorg. Chem.* **1980**, *19*, 956.
- [85] Y. You, X.-L. Wu, Y.-X. Yin, Y.-G. Guo, *Energy Environ. Sci.* **2014**, *7*, 1643.
- [86] D. Asakura, C. H. Li, Y. Mizuno, M. Okubo, H. Zhou, D. R. Talham, *J. Am. Chem. Soc.* **2013**, *135*, 2793.
- [87] A. Eftekhari, *J. Power Sources* **2004**, *126*, 221.
- [88] X. Bie, K. Kubota, T. Hosaka, K. Chihara, S. Komaba, *J. Mater. Chem. A* **2017**, *5*, 4325.
- [89] Z. Shadike, D.-R. Shi, W. Tian, M.-H. Cao, S.-F. Yang, J. Chen, Z.-W. Fu, *J. Mater. Chem. A* **2017**, *5*, 6393.
- [90] Q. Zhao, J. Wang, Y. Lu, Y. Li, G. Liang, J. Chen, *Angew. Chem.* **2016**, *128*, 12716.
- [91] X. Wu, Z. Jian, Z. Li, X. Ji, *Electrochem. Commun.* **2017**, *77*, 54.
- [92] M. S. Whittingham, *Chem. Rev.* **2004**, *104*, 4271.
- [93] M. H. Han, E. Gonzalo, G. Singh, T. Rojo, *Energy Environ. Sci.* **2015**, *8*, 81.
- [94] C. Delmas, C. Fouassier, P. Hagenmuller, *Physica B+C* **1980**, *99*, 81.
- [95] X. Wang, X. Xu, C. Niu, J. Meng, M. Huang, X. Liu, Z. Liu, L. Mai, *Nano Lett.* **2017**, *17*, 544.
- [96] A. K. Padhi, K. S. Nanjundaswamy, J. B. Goodenough, *J. Electrochem. Soc.* **1997**, *144*, 1188.
- [97] Z. Gong, Y. Yang, *Energy Environ. Sci.* **2011**, *4*, 3223.
- [98] C. Masquelier, L. Croguennec, *Chem. Rev.* **2013**, *113*, 6552.
- [99] N. Recham, G. Rousse, M. T. Sougrati, J.-N. Chotard, C. Frayret, S. Mariyappan, B. C. Melot, J.-C. Jumas, J.-M. Tarascon, *Chem. Mater.* **2012**, *24*, 4363.
- [100] S. S. Fedotov, N. R. Khasanova, A. S. Samarin, O. A. Drozhzhin, D. Batuk, O. M. Karakulina, J. Hadermann, A. M. Abakumov, E. V. Antipov, *Chem. Mater.* **2016**, *28*, 411.
- [101] K. Chihara, A. Katogi, K. Kubota, S. Komaba, *Chem. Commun.* **2017**, *53*, 5208.
- [102] V. Mathew, S. Kim, J. Kang, J. Gim, J. Song, J. P. Baboo, W. Park, D. Ahn, J. Han, L. Gu, Y. Wang, Y.-S. Hu, Y.-K. Sun, J. Kim, *NPG Asia Mater.* **2014**, *6*, e138.
- [103] J. Han, G.-N. Li, F. Liu, M. Wang, Y. Zhang, L. Hu, C. Dai, M. Xu, *Chem. Commun.* **2017**, *53*, 1805.
- [104] Z. Xing, Z. Jian, W. Luo, Y. Qi, C. Bommier, E. S. Chong, Z. Li, L. Hu, X. Ji, *Energy Storage Mater.* **2016**, *2*, 63.
- [105] Z. Jian, Y. Liang, I. A. Rodríguez-Pérez, Y. Yao, X. Ji, *Electrochem. Commun.* **2016**, *71*, 5.
- [106] K. Nakahara, J. Iriyama, S. Iwasa, M. Suguro, M. Satoh, E. J. Cairns, *J. Power Sources* **2007**, *165*, 398.
- [107] R. J. Clément, P. G. Bruce, C. P. Grey, *J. Electrochem. Soc.* **2015**, *162*, A2589.
- [108] K. Amine, H. Tukamoto, H. Yasuda, Y. Fujita, *J. Electrochem. Soc.* **1996**, *143*, 1607.
- [109] A. Jain, G. Hautier, S. P. Ong, C. J. Moore, C. C. Fischer, K. A. Persson, G. Ceder, *Phys. Rev. B* **2011**, *84*, 045115.